

Chemical Vapour Deposition of N/C/H Plasmas

Jason Pattle

Contents

1	Abstract	2
2	Introduction	3
2.1	Chemical Vapour Deposition	3
2.2	Nitrogen	7
3	Experimental	8
3.1	The Reactor	8
3.2	Reactor Conditions	9
3.2.1	Flow Rate and Ratio Experiments	11
3.2.2	Power experiments	11
3.2.3	Pressure Experiments	11
3.2.4	Profile Experiments	11
3.3	Spectroscopic Techniques	12
3.3.1	Cavity Ring-Down Spectroscopy	12
3.3.2	Optical Emission Spectroscopy	12
3.4	Computational Details	13
4	Results and Discussion	14
4.1	Experimental Results	14
4.1.1	CRDS For N ₂ As An Input Gas	14
4.1.2	CRDS For NH ₃ As An Input Gas	17
4.1.3	OES For N ₂ As An Input Gas	20
4.1.4	OES For NH ₃ As An Input Gas	29
4.2	Computational Results	34
4.2.1	NH Radical Incorporation	34
4.2.2	CN Radical Incorporation	38
5	Conclusion	41
	References	45

1 Abstract

Microwave plasma activated chemical vapour deposition (MPCVD) is studied with respect to nitrogen, carbon and hydrogen plasmas. Experiments that study the variations in the gas phase composition when changing variables such as; position above the substrate, microwave power, pressure and input gas concentration are carried out using two spectroscopic techniques. These techniques are optical emission spectroscopy (OES) and cavity ring-down spectroscopy (CRDS). These experiments are carried out on plasmas that are created using nitrogen (N_2) and ammonia (NH_3) as the nitrogen containing input gases. The other gases within the mixture are methane (CH_4) and hydrogen (H_2). These experiments show that the use of NH_3 as an input gas significantly increases the active nitrogen content of the plasma with respect to the use of N_2 . Other results show evidence for competing reactions within the plasma such as the competition between CN and NH species and the competition between CN and other carbon species such as C_2 and CH . Computational studies are also carried out using two density functional theory (DFT) basis sets; B3LYP/6-31G(d) and B3LYP/6-311G(d,p). These studies look at the chemistry of nitrogen containing radicals at the substrate surface in a CVD environment. Energies of optimized small diamond structures (using C_9H_{14} as a starting point) as well as activation energies for reactions between these structures are presented. These show that there are several possible routes for the incorporation of nitrogen into the growing diamond surface. These incorporation reactions involve non-carbon containing surface radicals such as S-NH and S-N where S is a surface carbon. Other incorporation routes are available for carbon containing surface radicals such as S-CNH and S-CN. Other implications from the computational studies show that surface species that differ by terminating hydrogen atoms such as S-N, S-NH and S-NH₂ as well as S-CN and S-CNH are related in equilibrium by the abstraction and termination reactions with atomic hydrogen in the plasma.

2 Introduction

This report discusses chemical vapour deposition (CVD) with respect to input gases containing nitrogen. This section introduces chemical vapour deposition as a technique as well as the interest for the study of nitrogen.

2.1 Chemical Vapour Deposition

CVD of diamond is a well established field of research that started in 1962 with William G. Eversole publishing the first ever results [1]. This method differed from the methods for diamond growth at the time by using relatively low pressures and temperatures with respect to other methods. A notable method for diamond growth that is not CVD is a high pressure, high temperature method (HPHT). HPHT methods typically apply temperatures exceeding 1700 K and pressures provided by hydraulic anvils to high purity carbon sources in order to create diamond. Under low pressure and temperature conditions in CVD diamond growth, diamond is metastable with respect to graphite. This translates to an effect where any form of carbon grown that does not show a cubic arrangement will either be re-arranged into a cubic arrangement or removed from the growing surface. This leads to an effective method for the growth of diamond films of thicknesses varying from the millimetre to nanometre range [2]. The technique for diamond growth that is focused on in this paper is microwave plasma-enhanced chemical vapour deposition (MPCVD). This technique uses a gas mixture that consists of carbon and hydrogen, often CH_4/H_2 , to grow diamond. Other carbon containing gases can be used but research has shown that diamond CVD growth is sensitive to C/H ratio but is largely independent of carbon source gas [2] [3].

The common conditions for diamond growth in such a reactor are as follows; pressures (p) of 150 torr, microwave powers (P) of 1.5 kW leading to gas temperatures ranging from 300 K at the outer regions of the CVD reactor to 3000 K towards the centre of the plasma. The source gases previously discussed have their concentration determined by the flow rate of the respective gas in comparison to the total flow rate. The flow rate of a gas is the rate at which the volume of the gas enters the reactor. The standard total flow rate used is 500 standard cubic centimetres per minute (sccm) [2]. Therefore a concentration of 4% CH_4 and 96% H_2 corresponds to flow rates of 20 sccm and 480 sccm respectively.

The method by which a plasma is used to enhance the chemical deposition process is by the excitation of the main input gas discussed above, H_2 . MPCVD typically uses between 1 to 2% of the power that is introduced in the form of microwaves to dissociate H_2 depending upon other conditions within the reactor [4]. The majority of the remaining input power has been found to excite H_2 rotationally and vibrationally. Collisions between species that exist within the plasma quench the excitation of H_2 leading to highly kinetically excited species in the plasma. This increases the overall temperature of the plasma. Many other reactions occur within a MPCVD plasma. These reactions include dissociation reactions which split molecules introduced in the input gases into various species, and recombination reactions which recombine the species that are produced into larger molecules. Any species formed in this manner can be excited kinetically (as previously discussed), electronically, and for molecules vibrationally and rotationally. This allows for a variety of detection methods including the two used in this report; cavity ring-down spectroscopy which uses electronic absorption to detect the presence of species and optical emission spectroscopy which

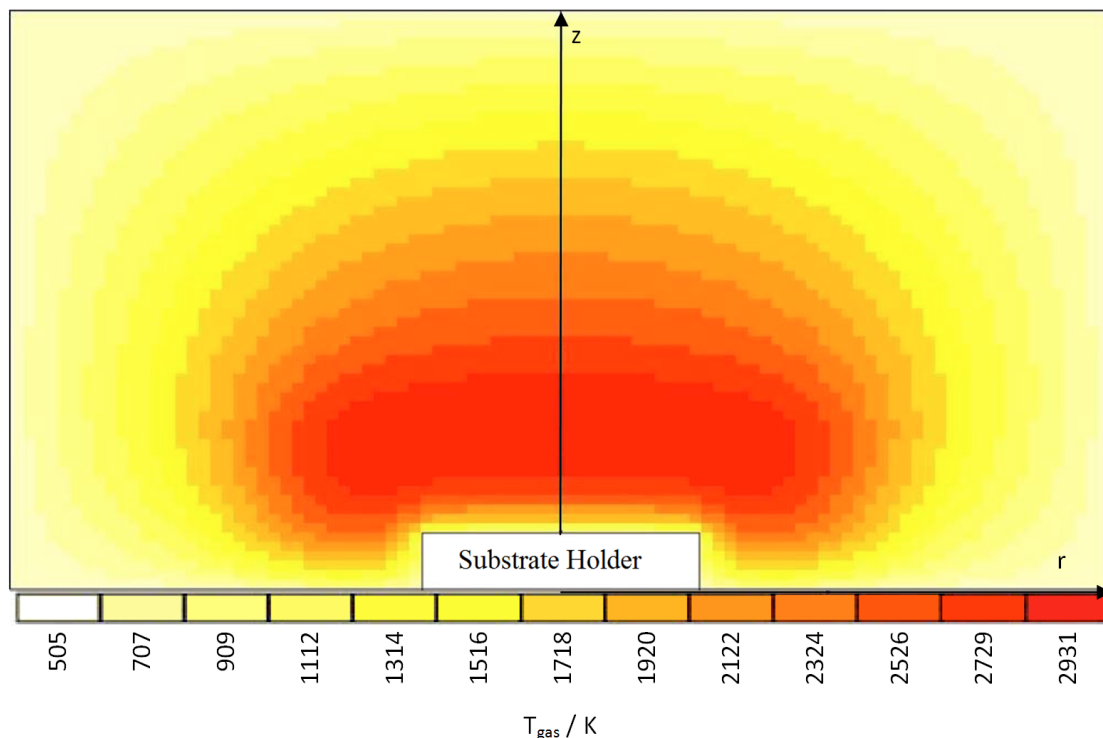


Figure 1: Adapted from Mankelevich, Ashfold and Ma [4]. A 2D colour plot depicting the calculated gas temperature, T_{gas} , in kelvin as a function of position within the reactor. Input power $P = 1.5$ kW, pressure $p = 150$ Torr, substrate holder diameter $d = 3$ cm. Note the cylindrical symmetry about the z axis

detects the emissions from excited species within the plasma. Perhaps the most important excited species within the plasma are hydrogen atoms. This is due to their reaction with the diamond surface. Due to the fact that there is a high percentage of atomic hydrogen within the plasma (8%) there are a high number of collisions between gas phase H atoms and surface carbon sites. These frequencies vary from 10^4 to 10^7 Hz per surface carbon site depending on CVD method and conditions [5]. Typically for the plasmas discussed in this report the frequencies are closer to 10^7 . Collisions between atomic hydrogen and surface carbon sites serve to hydrogenate the diamond surface which, in turn, prevents the growth of graphite allowing diamond to become metastable. Therefore all carbon sites have a high probability of being terminated by hydrogen. The reaction mechanism for a surface site undergoing termination by hydrogen can be seen in equation 1. However, the surface collisions between hydrogen atoms in the plasma and surface sites also serve to abstract hydrogen from sites that are already terminated leading to a surface radical site, S. This can be seen in equation 2.



$$f_S = \frac{k_1}{k_1 + k_2} \quad (3)$$

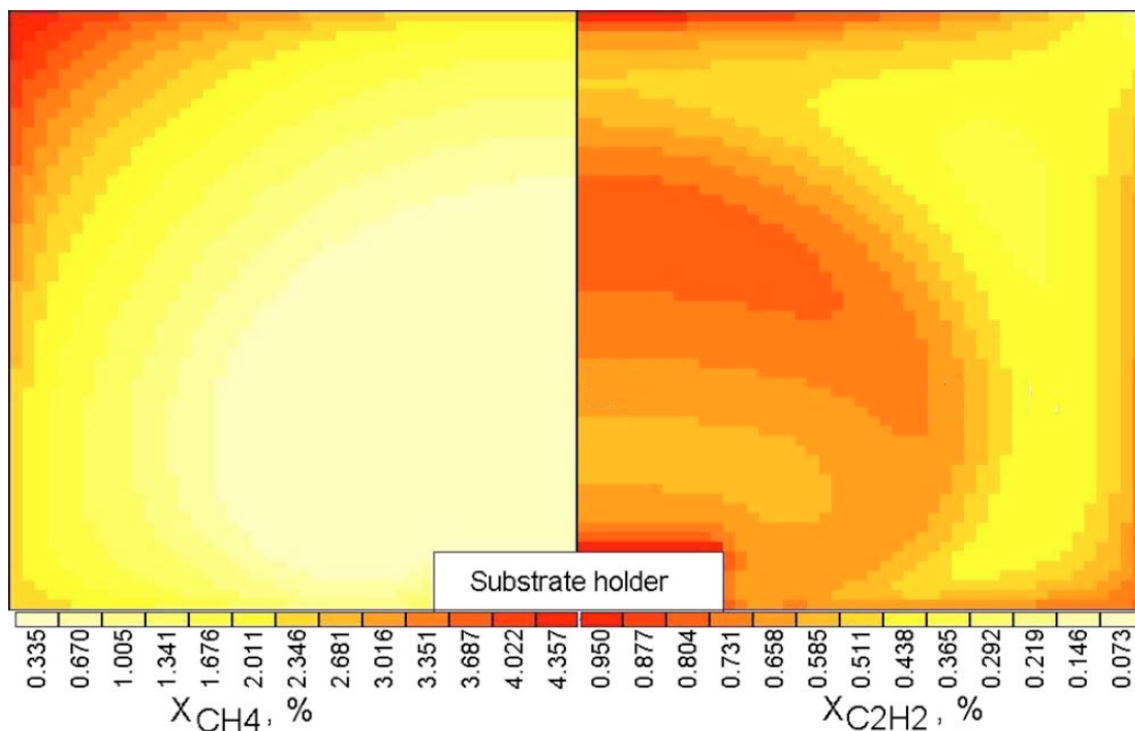


Figure 2: Adapted from Mankelevich, Ashfold and Ma [4]. A 2D (r, z) colour plot of the methane (left) and acetylene (right) distribution in the reactor. The plots show the molefraction as a percentage of total gas given by the standard conditions; $p = 150$ Torr, $P = 1.5$ kW, 4.4% CH_4 / 7% Ar / 88.6% H_2

Calculations have been made to predict the steady state surface radical coverage [6]. This has led to equation 3 which relates the rate constants of reactions 1 and 2 to the surface coverage, f_s . At surface temperatures between 1100 and 1500 K equation 3 predicts surface coverages between 0.12 and 0.37 [6]. These values are based on the fact that with each collision of a hydrogen atom with the surface there is a related probability for hydrogen abstraction and addition. The probability of addition to a surface radical site is close to 1, this is because the process is exothermic since a S-H bond is formed and no bonds are broken. The case for abstraction however is different with a probability closer to 0.1. This means that surface carbon sites are frequently having terminated hydrogen atoms abstracted and, essentially instantaneously, re-terminated. This gives a lifetime of about $0.1 \mu s$ for a surface radical site. Rate constants of reactions that can occur at the surface are limited if the surface adduct is not a stable surface species. This is because, if the reaction does not occur in a sufficient time, it is likely that it will become abstracted by collision with atomic hydrogen.

The surface radical sites discussed above can undergo reactions with other species that exist within the plasma. For the case of diamond growth by MPCVD, carbon containing gases provide carbon containing radicals that add to the surface. These carbon containing radicals then incorporate to form stable surface species where the process is then repeated. This is the mechanism by which diamond is grown. The carbon containing source gas undergoes many reactions within the plasma. Some of these reactions serve to increase or decrease the hydrogen termination of the carbon radical.

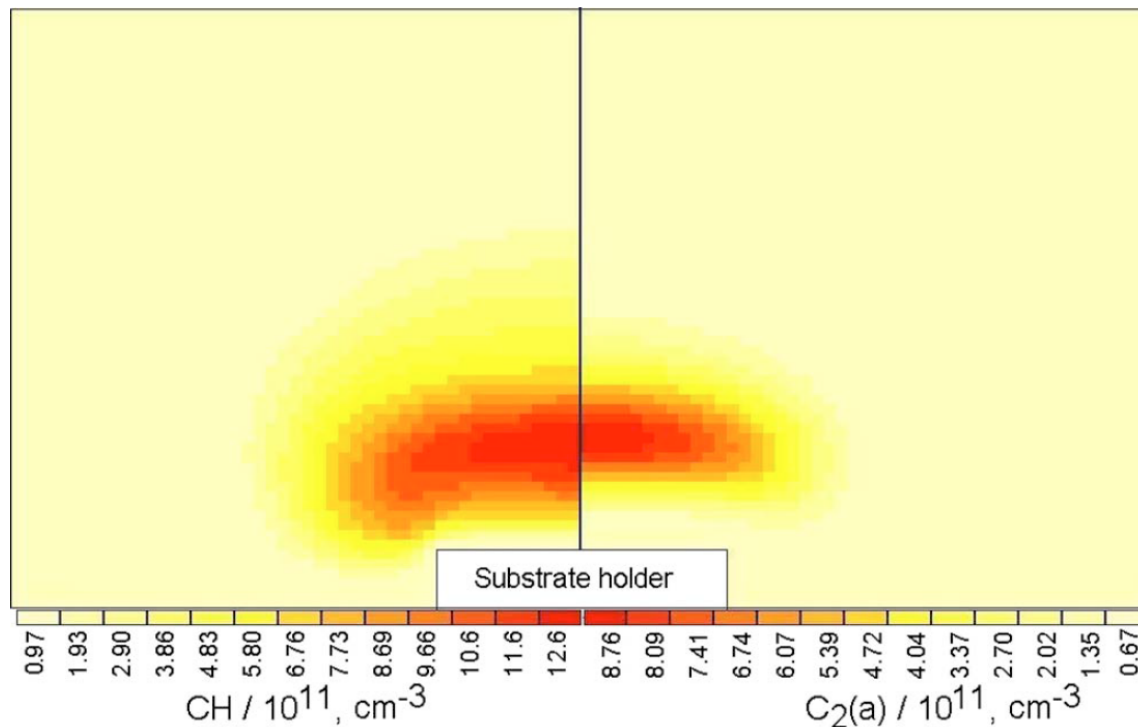
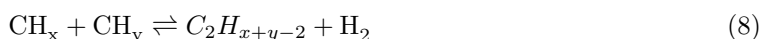


Figure 3: Adapted from Mankelevich, Ashfold and Ma [4]. A 2D (r, z) colour plot of the CH radical (left) and C_2 radical (right) distribution in the reactor. The plots show the number densities of these radicals under standard conditions discussed in (Figure 2)

These are called 'H-shifting' reactions which follow the forms seen in equations 4 and 5 where $x=1$ to 4 [2].



Reactions that form acetylenic (C_2H_x) species also occur within the plasma. These form larger species, the reactions for which can be seen in equations 6, 7 and 8 [2]. Some examples of the species that these five reactions can produce are CH, C_2 and C_2H_2 . CH_4 is also found within the plasma, it can be an unreacted molecule from the input gas mixture or it can be formed from 'H-shifting' or recombination reactions. The variation of the temperature throughout the reactor can be found in figure 1. It is observed that the centre of the plasma, which is the hottest region of the plasma, occurs at a height of 8 mm above the substrate. Due to this spatial distribution of the temperature the radicals given as examples previously also show a spatial distribution. This is because these reactions have different activation energies and reaction enthalpies. The spatial distributions of these radicals can be observed in figures 2 and 3. It can be seen in figure 2 that CH_4 is found in

the outer regions of the plasma, this shows that it is broken down in the hotter regions of the plasma to form other species. C_2H_2 is also found over the whole reactor due to combination reactions. The species most likely responsible for diamond growth is CH_3 . CH and C_2 are spectroscopically active and therefore are easily probed in CVD plasmas. The distribution of these two species, seen in figure 3, can be used to predict the distribution of CH_3 . The calculated points of highest CH_3 concentration within the plasma occur in the regions intermediate temperature. This gives a 'shell' of CH_3 directly around the distribution of CH seen in figure 3. This brings a significant concentration of CH_3 close to the substrate surface allowing a high number of collisions with the surface [4].

The carbon species previously discussed that exist within the plasma are responsible for the growth of diamond by the following general mechanism: The species undergoes collisions with the surface and can react if they collide with a surface radical site. These form surface adducts that can follow two mechanisms, one is to become abstracted by atomic hydrogen that collides from the plasma, the other is to become incorporated into the surface by a series of steps that involve a general ring opening and closing step. This process produces stable species and has been presented by several authors [2] [7] [8].

2.2 Nitrogen

Addition of various gases to the input gas mixture can have a variety of effects on growth rate, morphology and quality of grown diamond. The addition of nitrogen is of interest to the semiconductor industry as nitrogen-doped diamond is a *n*-type semiconductor [9]. However the use of nitrogen-doped diamond as a *n*-type semiconductor is limited due to the fact that it is not a good semiconductor compared to the *p*-type semiconductor formed when diamond is boron doped.

It has been found that, in plasma jet CVD, the growth rate is affected quite substantially by variations in nitrogen content in the input gas [9]. The growth rate has been observed to double when the N_2/CH_4 ratio is increased from 0.5 to 3.5% [9]. This effect is also observed in the context of a microwave activated plasma reactor. The growth rate has been observed to increase by many authors [10] [11] [12] and therefore the study of both gas and surface chemistry under the influence of added nitrogen is of interest. The influence of nitrogen on the growth of [100] and [111] faces is different, for example the concentration of nitrogen in [111] faces are greater than in [100] faces [10]. This suggests that the mechanisms of growth are different on the different planes.

The increased growth rate is not the only motivation for the study of nitrogen gas addition. Nitrogen is the most common impurity found in CVD diamond [12]. This is most likely due to any impurities in input gas or possibly due to any leaks into the reactor. These impurities give a yellow tarnish to the diamond grown and reduce properties such as the optical transparency and thermal conductivity [9]. It was found by Samlenski *et al.*, using nuclear reaction analysis to quantitatively determine the ^{15}N isotope impurity, that $CH_4/H_2/N_2$ reaction mixtures with a N/C ratio of 2% result in 4 ppm ([100]) and 13.5 ppm ([111]) of nitrogen incorporated in the CVD diamond film [13]. This preference for [111] plane incorporation gives evidence for the previously discussed mechanism difference between planes. This gives motivation for the computational research carried out in this report to study the incorporation mechanisms for nitrogen containing radicals into the surface.

CVD experiments have been carried out by various authors in hot filament (HF) reactors [14] [15]. These experiments observe changes in both the diamond grown and the gas phase chemistry that accompanies diamond growth. The aim of this series of experiments is to study the gas phase chemistry that occurs in the plasma of a MPCVD reactor during CVD growth. Some studies have been carried out on the gas phase chemistry present in a MPCVD reactor [16]. These studies have shown the detection of nitrogen containing radicals such as CN by optical emission spectra (OES) as well as the effects on carbon containing radicals as functions of nitrogen content. The spatial distribution of radicals has also been studied close to the substrate surface. This report will expand upon the data already found for nitrogen additions to a CVD gas mixture by assessing the change in gas phase composition with other variables, including the power and pressure. The data already found for spatial distributions of radicals will also be expanded upon by studying other nitrogen containing radicals such as NH as well as exploring different nitrogen containing input gases such as N₂ and NH₃. Different detection methods will also be used in this study. Cavity ring-down spectroscopy (CRDS) is a method by which the column density of a species can be found by the absorption of light produced by laser sources at specific wavelengths. Another technique that will be used is optical emission spectroscopy (OES) which studies the emission from species within the plasma.

3 Experimental

3.1 The Reactor

The MPCVD process which is discussed in section 2.1 was carried out within a CVD reactor. This reactor provided an environment in which a plasma can be created and maintained by the use of microwaves (MW) at powers that are varied for different experiments. A picture of the plasma that is created inside the reactor can be seen in figure 4(a). The details of this reactor have been presented elsewhere however a brief description will be outlined here [17] [18] [19]. A diagram of the reactor can be found in figure 5 which shows the configuration for both OES and CRDS experiments separately. The general form of the reactor is a cylindrical housing whose volume is approximately 600 cm³. This housing is aligned vertically so that there is cylindrical symmetry around the central vertical axis, Z. The housing can be evacuated to low pressures around 10⁻² Torr and then maintained at around 150 Torr when reaction gas mixtures are introduced into the housing by stainless steel inlet pipes. The flow rates of input gases are controlled by individual mass flow controllers which pre-mix the gases before entering the housing. The MW radiation is introduced through a quartz window at the top of the housing which is pointed towards a substrate holder at the bottom. The substrate used in this experiment was not changed as the growth of diamond is not the subject of interest for this report. The substrate holder is water-cooled on the base of the reactor to maintain constant substrate temperatures which are monitored by an optical pyrometer.

For CRDS measurements the viewing windows are replaced by flexible cylindrical stainless steel side arms. The flexibility of the side arms allow the plasma ball to be studied over a range of heights. At each end of the side arms high-reflectivity cavity mirrors are mounted (LayerTec, Inc. $R > 0.999$, planoconcave, 1 m radius of curvature) [17]. Light that is not reflected then enters the detector.

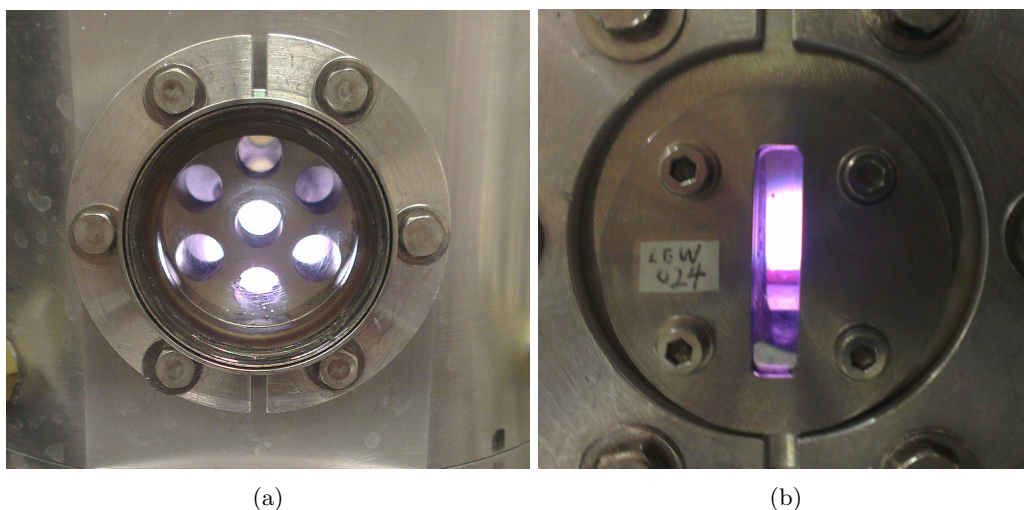


Figure 4: Two pictures of a plasma within the reactor housing. (a) shows a plasma through the viewing aperture for a reactor that is at standard conditions for a nitrogen, carbon and hydrogen plasma. (b) shows a plasma through the vertical viewing aperture which was used throughout all experiments and allows the detection of plasma species by CRDS or OES over a vertical length of approximately 25 mm.

For optical emission spectroscopy viewing slots are mounted on the side of the reactor. These consist of 25 mm(vert.) by 5.5 mm(horiz.) slot apertures which allow the position of measurement to be varied vertically [19]. This can be seen in figure 4(b). The light that comes from the reactor then is focused with a lens through an aperture into another lens so that a precise point within the plasma is imaged onto the detector. The detector consists of an optical fibre which leads to the spectrometer.

The position of the reactor is at a fixed height but the equipment used for OES and CRDS experiments can be moved vertically with an error of ± 0.05 mm. The measured height of the experiment is calibrated by making measurements either by OES or CRDS of an active plasma at decreasing height until no signal is observed. This is then the height of the substrate inside the reactor which is set to 0 mm. 25 mm above this height can be measured. The height of the apparatus is measured by a rigidly mounted Vernier scale.

3.2 Reactor Conditions

The data collection and spectroscopic techniques outlined in section 3.3 were used on a variety of conditions for nitrogen containing gases in order to study the variation in detection of various radicals within the CVD plasma. Different nitrogen containing gases were used in order to gain insight into how the input gas affects the various radical concentrations. The nitrogen containing gases used were: N_2 , NH_3 and a 1% N_2 : 99% H_2 gas mixture. The latter was used in order to

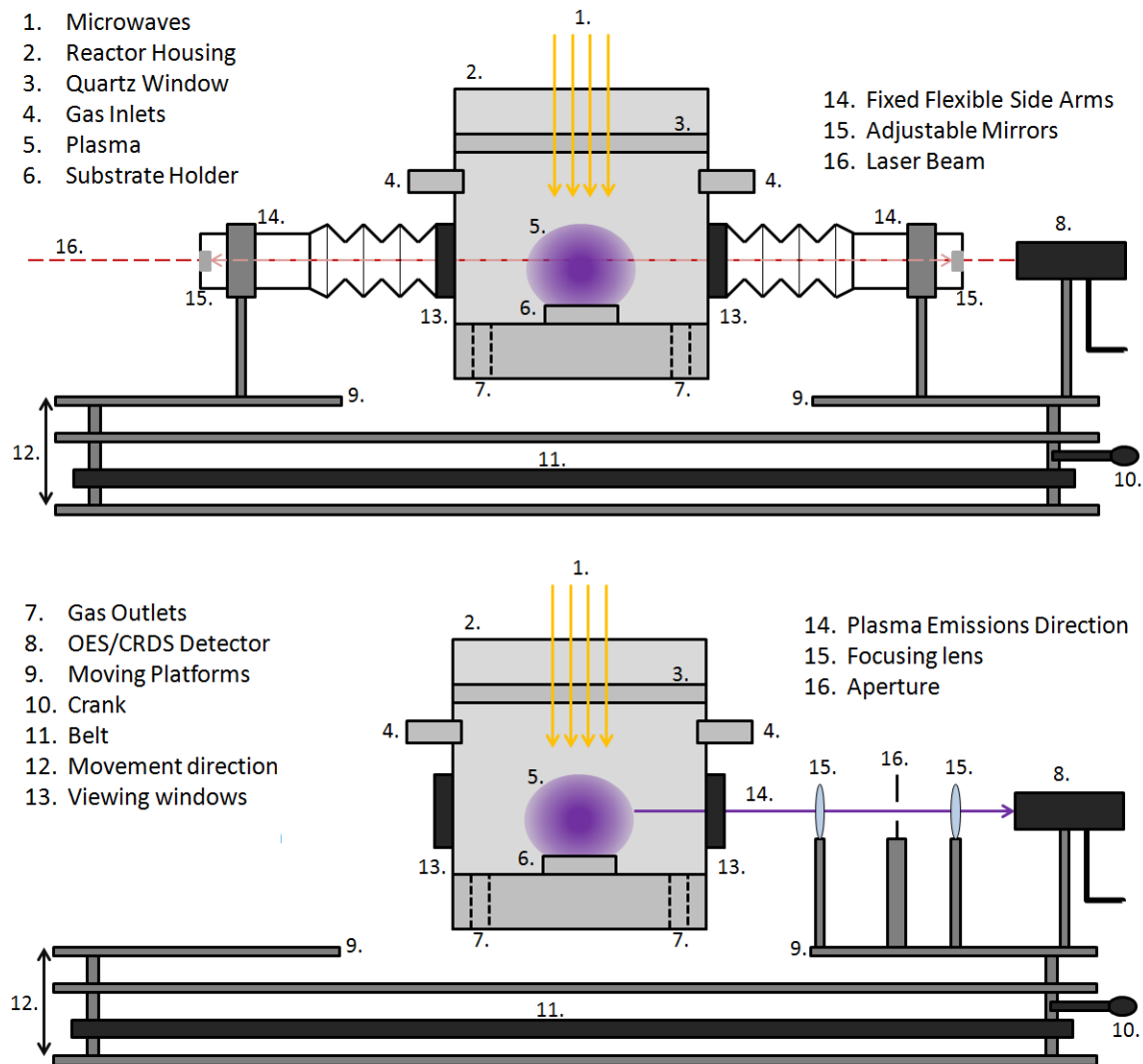


Figure 5: Adapted from Ma, Richley, Ashfold and Mankelevich [17]. Two schematics showing the layout of the CVD reactor for both CRDS (top) and OES (bottom) experiments. The legends on the left hand side numbered 1. through 13. apply to both schematics whereas the legends on the right hand side numbered 14. through 16. apply to their respective schematics (the top right legend applies only to the CRDS schematic, the bottom right legend applies only to the OES schematic).

reach parts per million (ppm) levels of N_2 as low as 100 ppm within the total gas flow. In all the spectroscopic experiments carried out in this report the total flow rate of the input gas mixture was kept constant at 500 sccm. The standard power used in the experiments in this report was 1.5 kW. The standard pressure used in the experiments in this report was 150 Torr. Another variable that was studied was the height above the reactor substrate labelled Z. The standard value of Z used was 8mm as this was the height at which the visible centre of the plasma is observed. The experiments that were carried out by varying the reactor conditions are detailed in the following

subsections.

3.2.1 Flow Rate and Ratio Experiments

In order to vary the concentration of the different input gases the flow rate of each was varied. For example if a gas mixture was to contain 6000 ppm N_2 , 40000 ppm CH_4 this would correspond to flow rates of 3 sccm N_2 and 20 sccm CH_4 . With the knowledge of the total flow rate at 500 sccm it can be calculated that the remaining 477 sccm would be H_2 giving rise to a $N_2/CH_4/H_2$ plasma with 954000 ppm of H_2 . One type of experiment carried out was the detection of radicals either by cavity ring-down spectroscopy or optical emission spectroscopy (detailed in section 3.3) whilst varying the ratio of input gases. These experiments are hereby referred to as ratio experiments, and the data set resulting will be referred to as ratio plots. Ratio experiments involve, for a two part plasma (e.g. a N_2/H_2 plasma), varying the concentration of both input gases and using a spectroscopic technique to measure radicals within the resulting plasma. For a three part plasma (e.g. a $N_2/CH_4/H_2$ plasma) ratio experiments have been carried out by varying the concentration of two input gases whilst keeping the third constant. For example a N_2 vs CH_4 ratio in a $N_2/CH_4/H_2$ plasma would vary the concentrations of N_2 and H_2 whilst keeping the concentration of CH_4 fixed.

3.2.2 Power experiments

Experiments that use spectroscopic techniques whilst varying the power and keeping other variables constant are referred to as power experiments. The data sets that result from these experiments are referred to as power plots. These experiments involve keeping the concentrations of all input gases, whether it is a two part or three part plasma, constant. Power experiments were run for a variety of input gases at a variety of input gas concentrations for both two and three part plasmas. The standard ranges of power studied in this report were from 0.5 to 1.8 kW. Some experiments involve studying other variables at high power. The power at which these experiments were carried out was 1.8 kW.

3.2.3 Pressure Experiments

Experiments that involve varying the pressure and keeping other variables constant are referred to as pressure experiments and the data collected as a result are referred to as pressure plots. The pressure is varied whilst keeping other variables constant. The standard ranges of pressure studied in this report were from 80 to 180 Torr. However some experiments involved either studying another variable at high pressure (300 Torr rather than the standard 150 Torr) or involved studying a pressure range centred at a higher value; 150 to 300 Torr.

3.2.4 Profile Experiments

Profiles involve varying the height above the reactor substrate whilst using spectroscopic techniques to obtain information about the plasma. The vertical range investigated is from the substrate surface through the plasma in the reactor up beyond where the plasma visibly ends. This is to detect

the spatial variety of radicals within the reactor. The standard range over which profiles are carried out is between 2 and 22 mm above the substrate.

3.3 Spectroscopic Techniques

Several techniques were used in conjunction with different spectroscopic techniques to obtain extensive experimental data about the plasma. The following outlines the details of each technique.

3.3.1 Cavity Ring-Down Spectroscopy

CRDS was used to study the adsorptions of NH radicals within the plasma. The reactor setup for CRDS can be seen in figure 5. For the CRDS spectra the laser setup was as follows: a Nd:YAG laser produces pulses of nanosecond length with a pulse frequency of 10Hz at 1064 nm, which is frequency doubled to 532nm. These pulses then use an LDS 698 dye to produce light at 672nm before being doubled to 336nm. These pulses were directed towards the reactor by using two 90 ° prisms. The height of the laser pulses was adjusted by having the upper most prism attached to the moving platforms. The laser pulses travel through the cavity arms attached to the reactor and are reflected by the mirrors to achieve ring-down. A photomultiplier tube is used as a detector which was placed behind a filter. The conversion of a CRDS signal into a column density is outlined in detail by many authors [15] [20] [21]. The frequency of the laser was varied using the tunable dye and a ring down signal was achieved for each. This signal was analysed by a custom written LABVIEW program which fitted a the logarithm of the ring down trace in order to obtain a ring down rate coefficient. The concentration was calculated from the ring down rate coefficient, length of the cavity ($L = 84$ cm) and absorption cross section radical studied.

3.3.2 Optical Emission Spectroscopy

OES was used to study emissions by species within the plasma. The reactor setup for OES can be seen in figure 5. The fibre optic cable then fed into a spectrometer which was cooled to 10 °C. The spectrometer was then calibrated using known spectra of fluorescent lights to the correct range of wavelengths. There were 2 wavelength ranges studied: a 280-580 nm range was used in order to study NH (336 nm), CN (388 nm), CH (431 nm) and C₂ (516 nm) radicals. A 380-680 nm range was used to compare the H (n=3) and H (n=4) to H(n=2) emissions (Balmer lines). Before each study a background was taken by leaving the optical fibre in place and turning off the plasma. Any spectra taken were then corrected by subtracting the background. In some cases the ambient light levels close to the fibre optic cable would change between a background being taken and a spectra being taken. This sometimes caused a negative spectrum to occur in places where features in the background spectrum had increased in amplitude. To avoid this the aperture that the emission light is focused through was decreased in size to stop as much of the background light entering as possible whilst still allowing the emissions to be collected. All spectra were taken as accumulative spectra over 32 runs at 0.05 second exposure times.

3.4 Computational Details

Computational experiments were carried out to give insight into the gas-surface chemistry between diamond and nitrogen radicals. Density functional theory (DFT) was used to optimize structures and calculate electronic energies of various surface species. These calculations were carried out using the Gaussian 03 program package. The method by which an accurate ground state energy was calculated was as follows: An optimization and frequency calculation was carried out using DFT with the basis set B3LYP/6-31G(d). This less accurate basis set was used to reduce the time taken to run a calculation as it provides a good balance between the computational demand and accuracy of the calculation. This basis set is appropriate for optimizing systems of size ranging from 21 to 26 atoms. To then accurately calculate the ground state energy of the optimized structure a higher basis set is used, namely B3LYP/6-311G(d,p). For these calculations the correct spin is chosen; either singlet, doublet or triplet, to reflect the electronic structure of the system. These methods of calculating the energy give a zero-point correction term which should be subtracted from the calculated energy to give the full electronic energy of the system. To calculate the energetics of a reaction mechanism the energy of the reactants is subtracted from the energy of the products to give the overall reaction energy.

Activation energies were also calculated for some species. This involves using a similar method as above to generate an optimized transition state species. This is done by using the same basis set as before. However instead of optimizing a single structure to a minimum, a starting structure and a final structure are used to optimize to a transition state using QST2.

An alternative method uses three structures; a starting structure, a final structure and an estimated transition state structure to optimize a transition state using QST3. This method is used when a QST2 method cannot converge to a transition state structure. For the QST2 and QST3 methods where the reactants are at a different spin to the products calculations were run setting the spin of the system to both the spin of the reactant and that of the product. If both spin methods produce a transition state structure the structure with the expected structure and the lowest ground state energy is taken. After the transition state structure has been optimized the energy is then calculated with the higher basis set as above. The activation energy is then simply calculated by subtracting the energy of the starting structure from the energy of the transition state. The activation energy shows the likelihood of a reaction at the surface proceeding. It is estimated that an activation energy approximately less than or equal to 100 kJ mol^{-1} is likely to proceed. Using a Arrhenius equation with a pre-exponential factor of 10^{13} s^{-1} (the vibrational frequency of a surface adduct) and this activation energy limit previously mentioned at surface temperatures of 1200 K this gives a rate constant of approximately 10^9 s^{-1} . This is a reaction rate that is 100 times faster than the collision rate of atomic hydrogen with a surface species which is 10^7 s^{-1} for a MPCVD plasma. This gives the reaction sufficient time to occur and therefore a reaction with an activation energy less than 100 kJ mol^{-1} is likely to occur.

Since both the DFT basis set functions are approximate methods there is an error associated with the above methods. Errors as large as 50 kJ mol^{-1} may be produced however it is unlikely that errors as large as this will occur due to error cancellation from several of the approximations used [7]. Therefore energies taken to the nearest 10 kJ mol^{-1} will best reflect the true energetics of the reaction.

The structures used in these optimization and energy calculations start with a C_9H_{14} diamond cluster that represents a C-C bond on a [100] diamond surface with 2×1 reconstruction. This starting structure has been used previously and calculations on larger diamond surface clusters using hybrid DFT/molecular mechanics (MM) methods suggest that it is appropriate to use the small C_9H_{14} cluster [7].

4 Results and Discussion

4.1 Experimental Results

This section presents and discusses the data obtained by carrying out experiments outlined in section 3.2 using the spectroscopic techniques outlined in section 3.3. Comparisons are made between the results from both cavity ring-down spectroscopy experiments and optical emission spectroscopy. Several references to active nitrogen are made. Active nitrogen is nitrogen within the plasma that exists in a state that is available to react and form nitrogen containing species. For example N_2 is not an active nitrogen species. Active carbon and active hydrogen refer to the same thing except for carbon and hydrogen respectively.

4.1.1 CRDS For N_2 As An Input Gas

This section discusses the data obtained from CRDS experiments using N_2 as the nitrogen containing input gas. This spectroscopic technique is detailed in section 3.3. The data presented is in the form of quantitative data for the column density of the $NH(v=0)$ radical. The column densities in this section are quoted to one decimal place. However the error on each column density is approximately 10% of the value.

Initially the nitrogen containing input gas studied was pure N_2 . The concentration of nitrogen in these plasmas were initially high in comparison to experiments carried out later for 1% N_2 in 99% H_2 input gas in section 4.1.3. Power, pressure, profile and ratio experiments were carried on two part plasmas (N_2/H_2), the results of these experiments can be seen in figures 6(a), 6(b), 6(c) and 7(a). Profile and ratio experiments were carried out on three part plasmas ($N_2/CH_4/H_2$), the results of these can be seen in figures 6(d) and 7(b).

Figure 6(a) is a power plot of a N_2/H_2 plasma at a N_2 concentration of 12000 ppm. It is studied over the standard range discussed in section 3.2.2. The plot shows a steady increase in the column density of NH with increasing power. The lowest value of the column density observed is $0.52 \times 10^{12} \text{ cm}^{-2}$ which quadruples to a value of $2.2 \times 10^{12} \text{ cm}^{-2}$ as the power increases from 0.8 to 1.8 kW. Since the NH concentration is proportional to the concentration of active nitrogen within the plasma this shows that as the power increases the active nitrogen content increases. Since the nitrogen containing gas in this case is N_2 the increase in power therefore must either; directly break the N_2 bond, cause H_2 to be broken at a higher energy allowing the H radicals to then cause the breaking of N_2 , or a combination of these two cases. The increase in NH radical column density in this plot suggests that N_2 as an input gas is not very efficient at producing active nitrogen. Hence, for the powers that were studied in this experiment, there will still be some N_2 left in the plasma

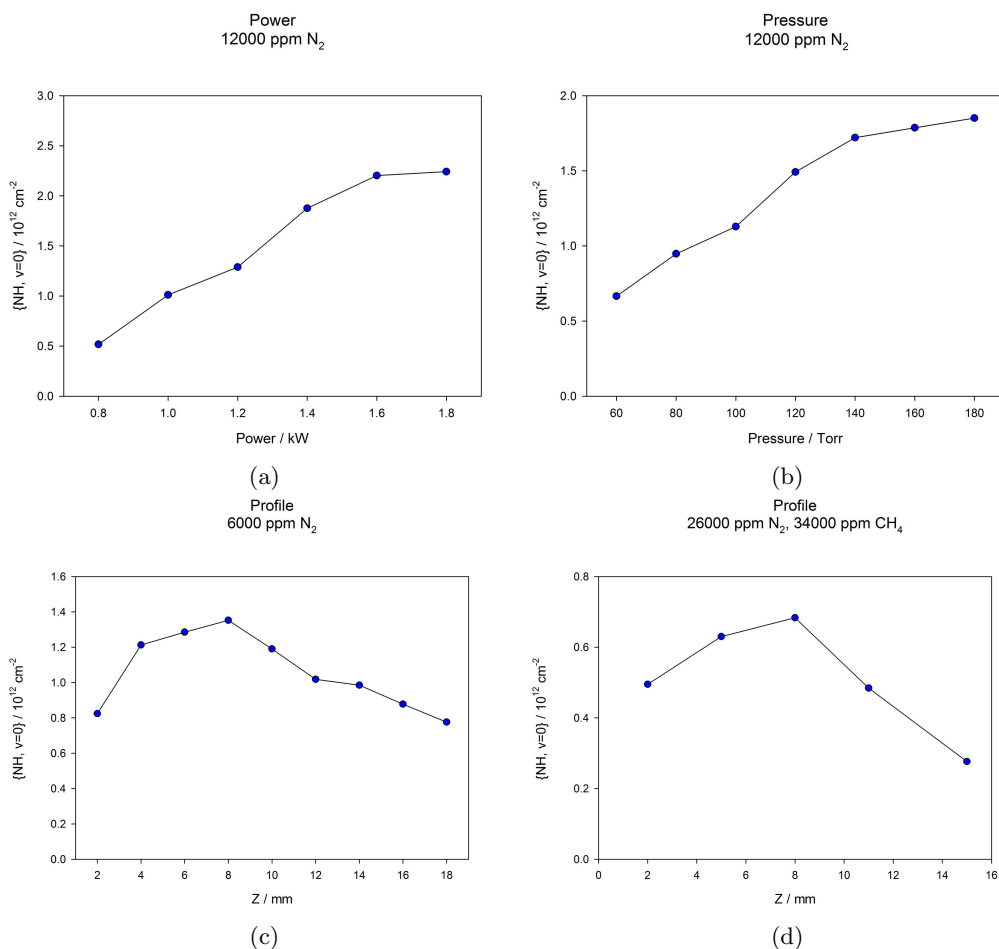


Figure 6: Four plots showing the results from four CRDS experiments. The measured parameter in each case is the column density of the $\text{NH}(v=0)$ radical. Units for each plot are shown beside the axes. (a) Shows a power plot of a N_2/H_2 plasma with 12000 ppm N_2 . (b) Shows a pressure plot of a N_2/H_2 plasma with 12000 ppm N_2 . (c) and (d) show profile plots for both; a N_2/H_2 plasma with 6000 ppm N_2 , and a $\text{N}_2/\text{CH}_4/\text{H}_2$ plasma with 26000 ppm N_2 and 34000 ppm CH_4 , respectively.

which have not undergone reactions to form other species. Therefore if higher powers were studied it would be expected that the NH radical column density would plateau at the point where the maximum power is used to dissociate N_2 and therefore is in equilibrium with active nitrogen in the plasma. Another reason for the increase of NH column density with increasing power is due to an increase in plasma size over this power range. Since the column density reflects the concentration contained along a path through the plasma at the point where it is studied an increase in plasma size would increase the column density. This must be taken into consideration when assessing trends for power plots.

Figure 6(b) is a pressure plot of a N_2/H_2 plasma at a concentration of 12000 ppm N_2 . It is studied over the standard range discussed in section 3.2.3. The plot starts at a similar value as figure 6(b) and again increases steadily. However it does not reach as high a value for the range studied. The maximum value measured is $1.9 \times 10^{12} \text{ cm}^{-2}$ at 180 Torr. The reason for the increase in NH column density is due to the fact that the total density of all gases increases with total pressure. Therefore there is a higher number of NH radicals observed. The pressure range studied here is relatively small and so at pressures greater than those studied the column density of NH would be expected to increase further. However at a sufficient pressure the column density should plateau since the maximum efficiency at which the microwaves can dissociate H_2 and therefore produce N_2 would be reached.

Figure 6(c) is a profile plot of a N_2/H_2 plasma at a concentration of 6000 ppm N_2 . It is studied over the standard range discussed in section 3.2.4. The general trend of this plot shows the expected shape for a profile plot. There is an initial low value for the column density of NH starting at $0.8 \times 10^{12} \text{ cm}^{-2}$ near the substrate. This value then increases with height until it peaks at a height of 8 mm above the substrate surface. This gives a peak column density of $1.35 \times 10^{12} \text{ cm}^{-2}$. The column density then decreases as the height increases. This shows that the conditions within the plasma at 8 mm above the substrate are most efficient at producing NH radicals. Alternatively this is the height at which reactions that remove NH radicals from the plasma are least efficient, for example recombination reactions that may instead produce N_2 or NH_x species which are not observed in this profile experiment. However since the temperature of the plasma at this height is at a maximum as shown by figure 1 recombination reactions are unlikely to occur. At heights other than the peak height of 8 mm the production of NH radicals becomes less efficient.

Figure 7(a) is a ratio plot of a N_2/H_2 plasma with varying N_2 and H_2 concentration. The range of concentrations of N_2 over which CRDS data was obtained is from 2000 to 40000 ppm N_2 which corresponds to a flow rate range of 1 to 20 sccm N_2 gas. As N_2 concentration is increased H_2 concentration is decreased so as to maintain a total flow rate of 500 sccm. The plot shows a steady increase of NH column density with increasing N_2 concentration. This result shows that the NH radical concentration within the plasma is proportional to the N_2 concentration when in an abundance of H_2 .

Figure 6(d) is a profile plot of a $N_2/CH_4/H_2$ plasma at 26000 ppm N_2 and 34000 ppm CH_4 . This corresponds to flow rates of 13 sccm N_2 and 17 sccm CH_4 leaving 470 sccm of H_2 . The concentration of N_2 used for this experiment is larger than that of the two part N_2/H_2 plasma experiments described above. This large concentration was chosen due to the fact that the CRDS signal that resulted from low N_2 concentration gave unreliable results due to the low column density of NH in the plasma. It can be seen that, compared to the profile of the two part, N_2/H_2 , plasma in figure 6(c), the column densities shown in figure 6(d) are much lower. The initial value at 2 mm above the substrate lies at $0.50 \times 10^{12} \text{ cm}^{-2}$ which follows the expected shape for a profile plot with a peak value at 8 mm of $0.68 \times 10^{12} \text{ cm}^{-2}$. The peak value in this case is lower than the lowest value for the N_2/H_2 plasma despite the use of an increased N_2 concentration. The reason for this difference in NH column density between the N_2/H_2 plasma profile plot and the $N_2/CH_4/H_2$ plasma profile plot is due to the fact that, with the addition of CH_4 , there are several reactions that active nitrogen, resulting from the input N_2 gas, can undergo with carbon. One such reaction is the production of CN which is studied by OES in sections 4.1.3 and 4.1.4. It should be noted that the

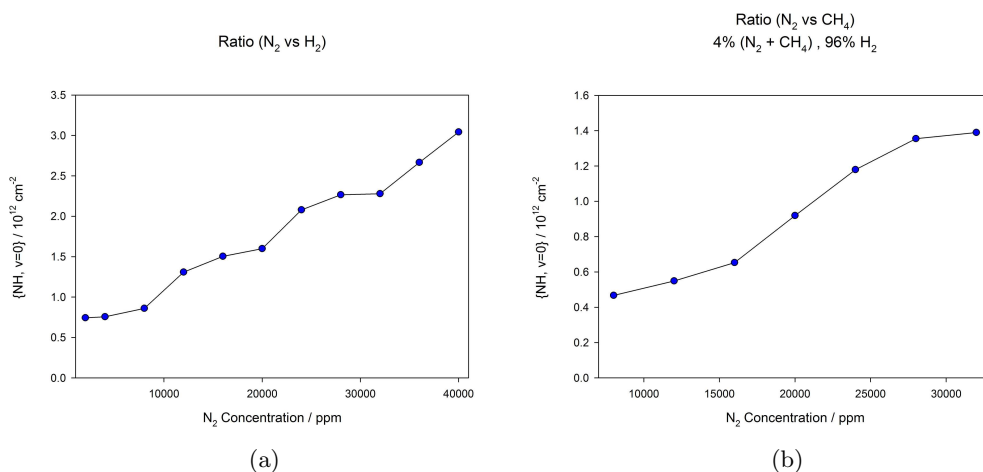


Figure 7: Two plots showing the results from two CRDS experiments. The measured parameter in each case is the column density of the $\text{NH}(v=0)$ radical. Units for each plot are shown beside the axes. (a) Shows a ratio plot of a N_2/H_2 plasma varying the N_2 concentration. (b) Shows a ratio plot of a $\text{N}_2/\text{CH}_4/\text{H}_2$ plasma varying the concentration of both N_2 and CH_4 but keeping the total concentration of $\text{N}_2 + \text{CH}_4$ at 4%.

additional hydrogen that can be liberated from the CH_4 molecules within the plasma make little difference to the NH_x reactions compared to the previous N_2/H_2 plasma cases. This is because the concentration of CH_4 is much less than the concentration of H_2 and therefore atomic hydrogen will be in abundance within the plasma in both cases.

Figure 7(b) is a ratio plot of a $\text{N}_2/\text{CH}_4/\text{H}_2$ plasma with varying N_2 and CH_4 concentrations whilst the concentration of H_2 remains constant. Both N_2 and CH_4 were studied over a concentration range of 8000 to 32000 ppm which corresponds to flow rates of 4 to 16 ppm. The total sum of the concentrations of N_2 and CH_4 was 40000 ppm throughout the experiment. Concentrations of CH_4 used in this experiment were less than the experiment above (figure 6(d)). This allows for the use of a lower concentration of N_2 to achieve a reliable CRDS signal. There is a steep increase in NH radical column density from the starting point where the concentration of CH_4 is at a maximum to the final point where it is then at a minimum. Two processes contribute to the increase in NH radical column density. The first of these is due to an increase in N_2 concentration which, as discussed above for figure 7(a), contributes to the increase in NH radical column density because of an increase in active nitrogen. The second is due to the decrease in CH_4 which contributes to the increase in NH radical column density due to the decrease in competing reaction routes that active nitrogen can undergo. This was discussed above when addressing figure 6(d).

4.1.2 CRDS For NH_3 As An Input Gas

This section discusses the data obtained from CRDS experiments using NH_3 as the nitrogen containing input gas. Data is presented in the same manner as in section 4.1.1.

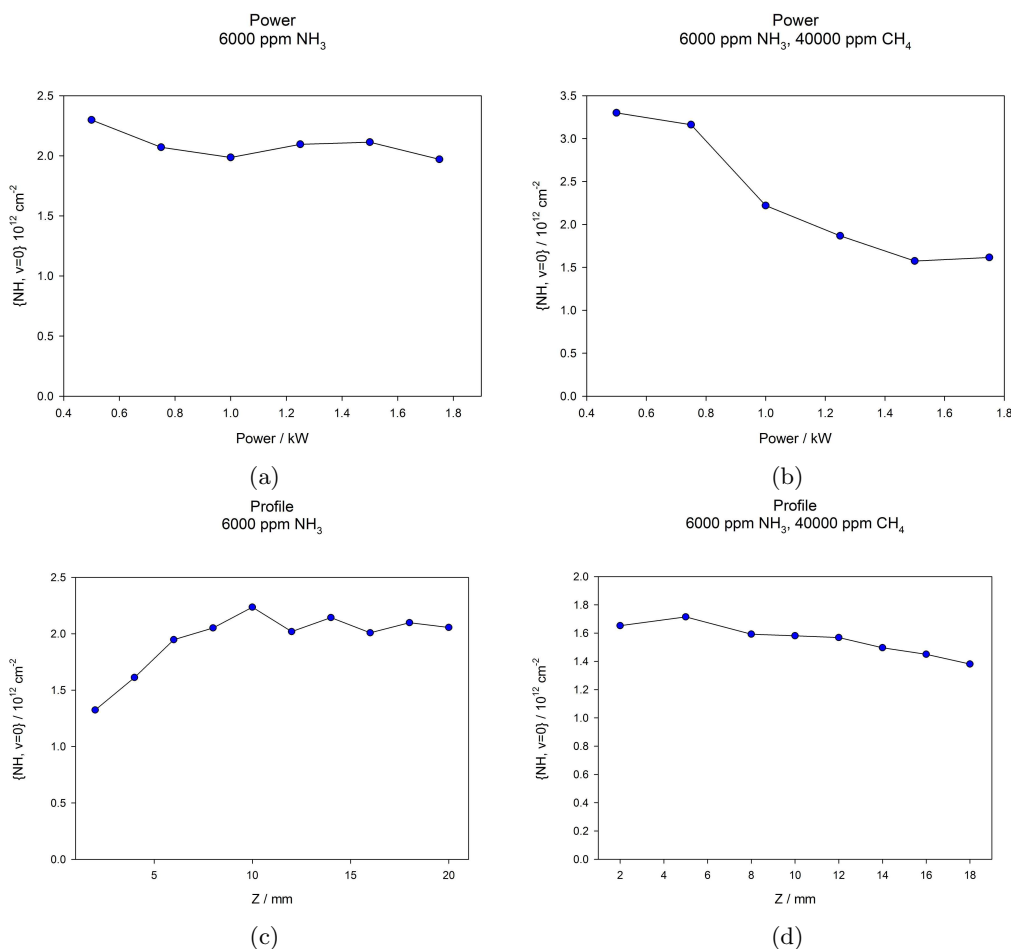


Figure 8: Four plots showing the results from four CRDS experiments. The measured parameter in each case is the column density of the $\text{NH}(v=0)$ radical. Units for each plot are shown beside the axes. (a) and (b) show power plots for both; a NH_3/H_2 plasma with 6000 ppm NH_3 , and a $\text{NH}_3/\text{CH}_4/\text{H}_2$ plasma with 6000 ppm NH_3 and 40000 ppm CH_4 , respectively. (c) and (d) show profile plots for both; a NH_3/H_2 plasma with 6000 ppm NH_3 , and a $\text{NH}_3/\text{CH}_4/\text{H}_2$ plasma with 6000 ppm NH_3 and 40000 ppm CH_4 , respectively.

Figures 8 and 9, which are discussed below, are power, profile and ratio experiments which were carried out using NH_3 as the nitrogen containing input gas. It should be noted that when comparing these figures with figures 6 and 7 the nitrogen content of the N_2 input gas experiment is double that of the NH_3 input gas for the same input gas flow rate due to the stoichiometry of the input gases.

Figures 8(a) and 8(b) show power plots for a NH_3/H_2 plasma and a $\text{NH}_3/\text{CH}_4/\text{H}_2$ plasma respectively. The concentration of NH_3 used in both these experiments was 6000 ppm and for figure 8(b)

the concentration of CH_4 used was 40000 ppm. Figure 8(a) shows that for increasing power the column density of the NH radical remains constant at a value of approximately $2.1 \times 10^{12} \text{ cm}^{-2}$. The absence of an increase in NH column density is due to the full conversion of NH_3 to active nitrogen which is in equilibrium with the NH radical. Comparing this to the case discussed above for figure 6(a) where there is an increase in NH radical concentration due to remaining N_2 molecules existing within the plasma shows that NH_3 is more efficient at producing active nitrogen. This is likely due to the fact that the N-N bond requires more energy to break than the N-H bonds within NH_3 . Therefore it is expected that any experiments carried out using NH_3 as an input gas rather than N_2 would result in a higher active nitrogen content within the plasma that is available to form species such as NH. This expectation is backed up by the fact that, for this experiment, at an input nitrogen content four times less than for figure 6(a) the NH column density is roughly 4 times larger for low powers. Figure 8(b) shows a decrease in NH column density with power. This is most likely due to an increase in power causing an increase in active carbon that reacts to form CN and other nitrogen and carbon containing species. This therefore decreases the concentration of NH radicals in the plasma by the fact that competing reaction routes will become more favourable.

Figures 8(c) and 8(d) show profile plots for NH_3/H_2 plasma and a $\text{NH}_3/\text{CH}_4/\text{H}_2$ plasma respectively. The concentration of NH_3 used in both these experiments was 6000 ppm however for figure 8(b) the concentration of CH_4 used was 40000 ppm. Figure 8(c) shows an initial increase in NH column density resulting in a maximum value of $2.23 \times 10^{12} \text{ cm}^{-2}$ at 10 mm above the substrate. This is then expected to decrease to follow a regular profile plot trend. However instead it plateaus around this maximum value. This could be because the range of values for the height above the substrate is not large enough to observe this drop in column density. If this were the case then the extended area over which NH is observed at high concentrations is most likely due to the large amount of active nitrogen as discussed above for figure 8(a). Figure 8(d) is approximately constant with height with a small drop off in NH column density at higher values. One explanation for the lack of a peak in NH radical density is that at the centre of the plasma, around 8 to 10 mm above the substrate, the conditions, such as temperature and electron temperature, favour reactions that produce radicals that are not observed in this experiment, such as CN or any NH_x species where $x \neq 1$.

Figures 9(a) and 9(b) show ratio plots for both H_3/H_2 and $\text{H}_3/\text{CH}_4/\text{H}_2$ plasmas respectively. Figure 9(a) is a ratio plot that varies the concentrations of both N_2 and H_2 for standard power, pressure and height. The range of concentrations studied for this figure is between 4000 and 20000 ppm N_2 . The general trend shows an increase in NH column density with increasing NH_3 concentration. This is the expected trend since the increase in active nitrogen will cause an increase in NH density in the same manner discussed for figure 7(a). Comparing figures 7(a) and 9(a) shows more evidence that NH_3 is more efficient at producing active nitrogen in the plasma as discussed for figures 8(a) and 8(b). This is evident due to the fact that under the same conditions, the NH column density for an N_2 input gas is approximately half the value of the NH column density for an NH_3 input gas. For example for the two figures 7(a) and 9(a) at 4000 ppm we observe a value of $0.7 \times 10^{12} \text{ cm}^{-2}$ for the N_2 plot and a value of $1.6 \times 10^{12} \text{ cm}^{-2}$ for the NH_3 plot. As the concentration of the nitrogen containing gas is increased to 20000 ppm we then observe a column density of $1.6 \times 10^{12} \text{ cm}^{-2}$ for the N_2 plot compared to a value of $3.0 \times 10^{12} \text{ cm}^{-2}$ for the NH_3 plot. Figure 9(b) shows the trend of the NH column density with increasing NH_3 concentration at a constant concentration of 6000 ppm CH_4 . The general trend is the same as for figure 9(a) in that with increasing NH_3 concentration the

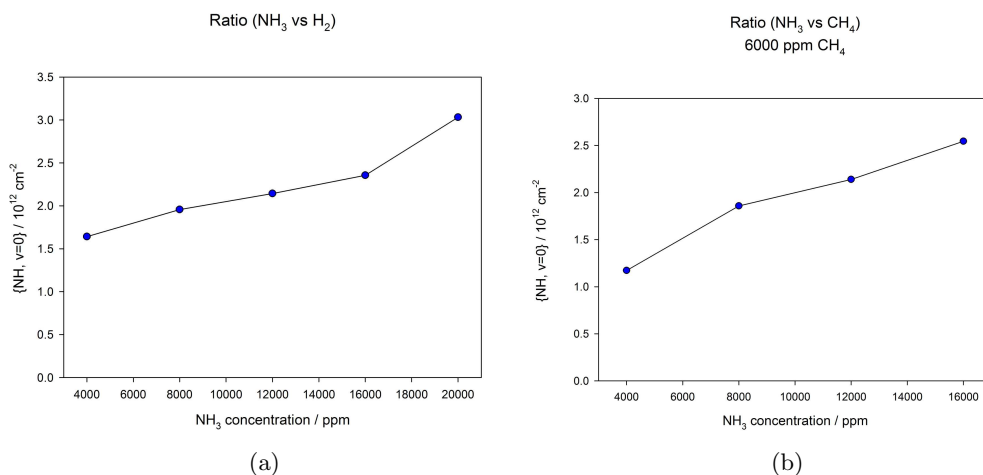


Figure 9: Two plots showing the results from two CRDS experiments. The measured parameter in each case is the column density of the NH(v=0) radical. Units for each plot are shown beside the axes. (a) Shows a ratio plot of a NH₃/H₂ plasma varying the NH₃ concentration. (b) Shows a ratio plot of a NH₃/CH₄/H₂ plasma varying the concentration of NH₃ while keeping the concentration of CH₄ at 6000 ppm.

column density of NH increases. However, as in previous experiments involving the addition of CH₄, the overall column density is lower due to competing reactions to form species such as CN and HCN.

4.1.3 OES For N₂ As An Input Gas

This section discusses the data obtained using OES. This spectroscopic technique is detailed in section 3.3. The data presented is in the form of qualitative relative amplitudes obtained by OES for the radicals; CN, CH, H (n=4), C₂, H (n=3) and NH. The measured variable for each plot is calculated by dividing the value for each point by the maximum value measured for the range studied. This gives relative amplitudes between 0 and 1, provided the amplitude measured from the optical emission spectrometer is positive in all cases. If a negative value occurs this will be due to an error in the measurement of the signal with respect to the background spectra, which is discussed in section 3.3. Note that because the OES technique gives relative amplitudes for each radical, quantitative analysis cannot be made between different radicals and different plots. Only qualitative comparisons can be made between the trends for each plot.

For two part plasmas, i.e. N₂/H₂ or NH₃/H₂ plasmas, the radicals that are measured are H (n=3), H (n=4) and NH in that order. For three part plasmas, i.e. N₂/CH₄/H₂ or NH₃/CH₄/H₂ plasmas, the radicals measured are CN, CH, H (n=4), C₂, H (n=3) and NH in that order. For some experiments the optical emission signal for NH was not strong enough to form reliable data in order to display in the respective plot. In these cases the data for NH has been omitted.

Initially both N₂/H₂ and N₂/CH₄/H₂ plasmas were studied using either N₂ gas or a 1% N₂ in 99%

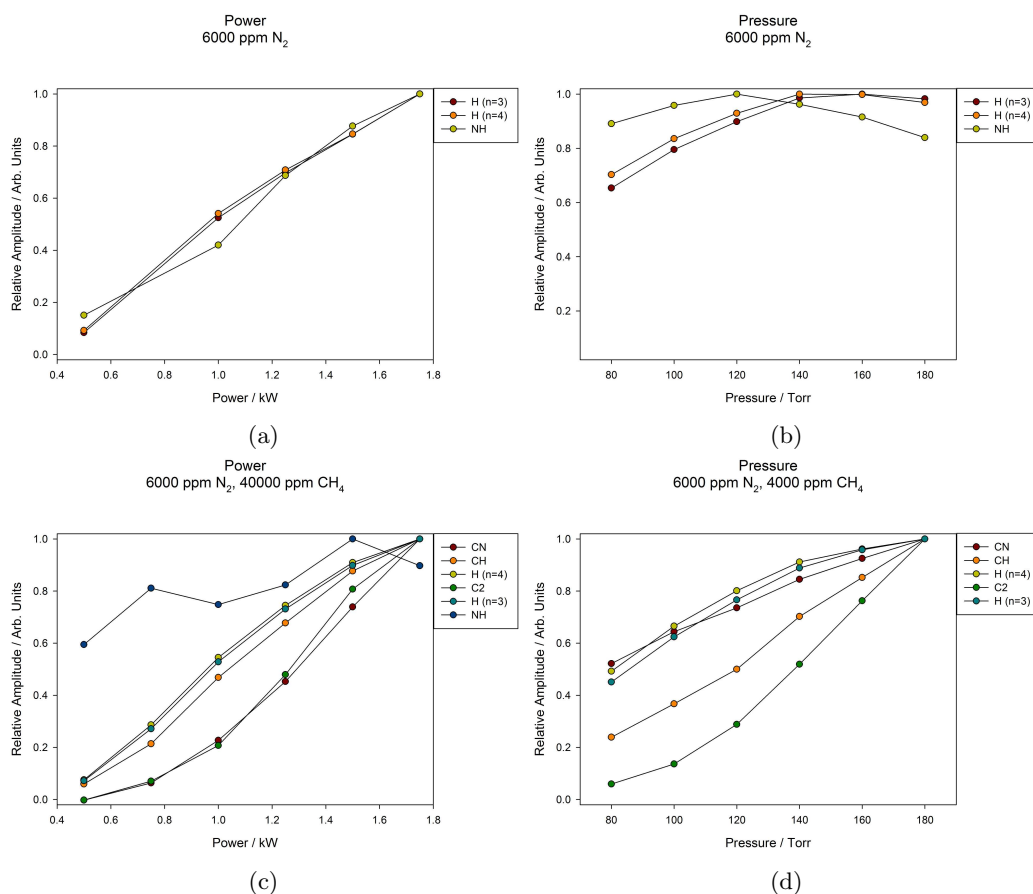


Figure 10: Four plots showing the results from four OES experiments. The measured parameter in each case is the relative amplitude which was calculated from the amplitude at each point divided by the maximum measured amplitude for each radical studied. Units for each plot are shown beside the axes and a legend for each data set within each graph is shown at the top right of each graph. (a) and (b) show power and pressure plots respectively of a N_2/H_2 at 6000 ppm N_2 . (c) Shows a power plot for a $N_2/CH_4/H_2$ plasma at 6000 ppm N_2 and 40000 ppm CH_4 . (d) Shows a pressure plot for a $N_2/CH_4/H_2$ plasma at 6000 ppm N_2 and 4000 ppm CH_4 .

H_2 gas mixture as the nitrogen containing input gas. This allowed the study of a range of different N_2 concentrations. Below the experiments involving the N_2 gas, i.e. the high N_2 concentration experiments, are discussed first followed by the low concentration experiments which used the 1% N_2 in 99% H_2 gas mixture.

Figure 10(a) and 10(b) show power and pressure plots respectively for two part, N_2/H_2 , plasmas. In each case the concentration of N_2 used was 6000 ppm. Both plots use the standard range for power and pressure plots discussed in section 3.2.2 and 3.2.3. The general trend for all radicals studied in figure 10(a) show an increase in relative amplitude with increasing power. The fact that H (n=3)

and H (n=4) show almost identical trends shows that, at the centre of the plasma, an increase in power increases the number of H₂ molecules which form excited H atoms. Therefore, crudely, increasing the power increases the total number of hydrogen radicals at any given time within the plasma. This increase in the number of excited H atoms increases the total energy of the system allowing N₂ molecules to dissociate on collision with H atoms forming more active nitrogen which will then go on to form different products within the plasma. One of these products is the measured NH radical. Therefore with the increase in energy absorbed by the system the number of observed NH radicals will increase due to an increase in the active nitrogen content of the plasma. This is agreed upon by the general trend shown by the NH radical in figure 10(a). Figure 10(b) shows the trends for the H (n=3), H (n=4) and NH radicals with increasing pressure. Again both H (n=3) and H (n=4) show the same trends, initially increasing and then levelling off at high pressures. This shows, as before, that there is an increase in the number of excited H atoms within the plasma. The NH radical trend, however, does not show an overall increase. Instead it shows an initial increase with a slight decrease at higher pressures. This initial increase follows the trends of the H (n=3) and H (n=4) radicals however as they start to level off the NH radical amplitude decreases. This trend is different to that shown by the column density of the NH radical seen in figure 6(b). The reason for the difference is due to the difference in technique used to measure this radical. CRDS is a technique that gives the absolute column density of the radical. An OES signal however is not as simple since the signal produced for any one radical depends upon both the concentration of the radical and the electron conditions within the plasma. If there is a higher electron density, or the electrons within the plasma have higher energy, collisions with radicals are more likely to result in the promotion to a radiative excited state. Therefore, a higher number of excited radicals leads to a larger emission and therefore a higher observed signal. The converse is also true for lower electron density or temperature. Therefore a decrease in NH signal here can be attributed to either a decrease in NH concentration or a decrease in the electron density or electron temperature. Since an increase in NH radical concentration is observed from CRDS experiments the contradicting trend shown here must be due to a decrease in electron density or electron temperature within the plasma.

Figures 10(c) and 10(d) show power and pressure plots respectively for three part, N₂/CH₄/H₂, plasmas. In each case the concentrations for N₂ and CH₄ were kept constant at 6000 ppm and 40000 ppm respectively. The trends for the power plot in figure 10(a) show a general increase in amplitude for all radicals with an increase in power. Some radicals such as C₂ and CN show a shallower increase with power than others. The reason for this is that, at the low energies that accompany the low powers, the reactions that form C₂ and CN are not energetically favourable compared to the reactions that form other products such as NH. Therefore initially there is no, or very little, observed C₂ or CN. This does not imply that the concentration of C₂ or CN within the plasma is non-existent since the detection by optical emission spectroscopy depends on a number of factors, such as temperature and electron gas temperature, that contribute to the emission from these radicals. The emission from H (n=3) and H (n=4) radicals show the same trend as with figure 10(a). This trend is also seen by the CH radical. The NH radical however does not show the same steep increase with power as in figure 10(a). This is because there are competing routes available to the N₂ input gas to follow that result in different nitrogen containing radicals. Figure 10(d) shows the trends for these radicals excluding the NH radical with increasing pressure. The NH radical in this case did not give sufficient reliable data over the range of pressures studied to show any trend and therefore was omitted from the pressure plot. All radicals studied in this plot show a general increase in detection by OES with pressure. This is due to the fact that as a higher

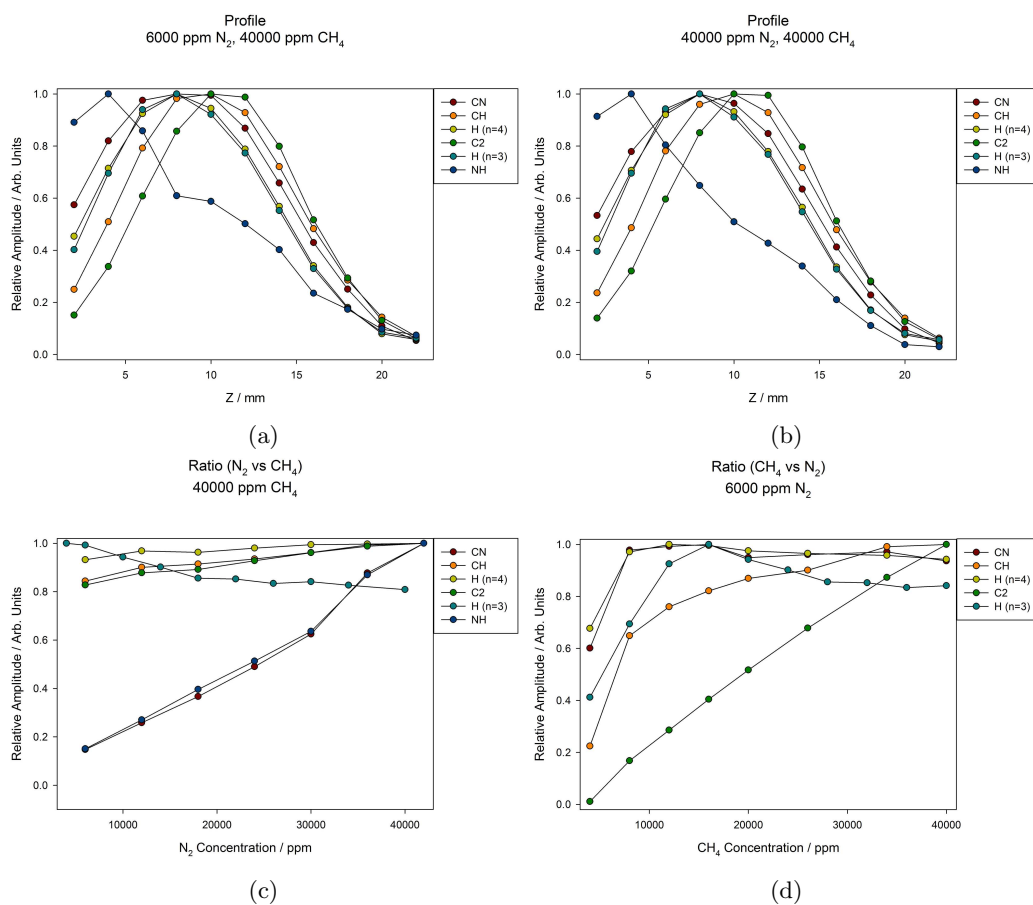


Figure 11: Four plots showing the results from four OES experiments. The measured parameter in each case is the relative amplitude which was calculated from the amplitude at each point divided by the maximum measured amplitude for each radical studied. Units for each plot are shown beside the axes and a legend for each data set within each graph is shown at the top right of each graph. (a) and (b) show profile plots for a N₂/CH₄/H₂ at 6000 ppm N₂ and 40000 ppm CH₄, and 40000 ppm N₂ and 40000 ppm CH₄ respectively. (c) Shows a ratio plot for a N₂/CH₄/H₂ plasma varying the concentration of N₂ whilst keeping the concentration of CH₄ constant at 40000 ppm. (d) Shows a ratio plot for a N₂/CH₄/H₂ plasma varying the concentration of CH₄ whilst keeping the concentration of N₂ constant at 6000 ppm.

pressure is introduced the amount active nitrogen increases due to the density of the input gases increasing.

Figures 11(a) and 11(b) show profile plots for N₂/CH₄/H₂ plasmas at two different concentrations of N₂. The first experiment was carried out at 6000 ppm N₂ and the second was carried out at 40000 ppm N₂. These plots show almost identical trends for all radicals studied. The trends shown

by all radicals follow expected profile shapes, that is; an initial increase with height to a maximum value after which a decrease is seen. The first to peak is the NH radical which peaks at 4 mm above the substrate surface. After this both the H (n=3) and H (n=4) atom emissions peak at 8 mm followed by the CN, CH and C₂ radicals which peak between 10 and 14 mm above the substrate surface. The difference between these peaks for different radicals stems from the reactions that occur within the plasma. The reason for a decrease in the NH peak and the CN peak is likely due to the competing reaction between the two, if the NH reaction were to require less energy than the competing CN reaction it could occur in cooler parts of the plasma, i.e. further away from the centre at 8 mm. Therefore closer to the higher temperature centre of the plasma the CN reaction would be dominant over the NH reaction therefore leading to an increase in the number of observed CN radicals towards the centre of the plasma with a decrease in the number of observed NH radicals. It should be noted that a number of factors should also be taken into consideration when observing OES data such as the fact that concentration of radicals is not the only contributing factor to the observed intensity. Other competing reactions similar to the two previously discussed here may also lead to the difference in peak height for the carbon containing radicals CN, CH and C₂. The H (n=3) and H (n=4) atoms peak in the centre of the plasma at 8 mm above the substrate surface. The NH peak for these cases disagrees with the observations made in section 4.1.1 in figure 6(d) which shows the peak value for the column density of NH to occur at 8 mm above the substrate surface. This is due to the difference in the methods for measuring an NH signal. CRDS measures the absolute column density for the NH radical within the plasma where as OES measures the emission from NH radicals in the plasma. There are a number of additional factors, rather than simply the concentration of NH radicals, in the plasma that contribute to the observed OES signal such as gas and electron gas temperature. A change in electron gas temperature is related to an increase in emissions from species within the species due to an increase in the number of collisions with sufficient energy to excite a species into a radiative site. Therefore it is not entirely reliable to compare trends between OES and CRDS measurements where there is a significant change in temperature within the plasma. It is well known that the temperature of the plasma changes spatially (see figure 1) and therefore profile measurements may not be compared accurately between OES and CRDS measurements [2].

Figures 11(c) and 11(d) show ratio plots for N₂/CH₄/H₂ plasmas. Figure 11(c) shows a ratio plot with varying N₂ concentration whilst keeping the concentration of CH₄ constant at 40000 ppm. As the concentration of N₂ is increased, the nitrogen containing radicals, CN and NH, both show an increasing trend. This is due to the effect discussed previously in which there is a greater concentration of active nitrogen that forms these two radicals. If the range of this plot was extended well beyond the concentration of CH₄ used then the trends of these two radicals would be expected to differ. For example the CN radical would be expected to plateau at a lower N₂ concentration than NH due to the fact that the concentration of CH₄ is limited. However the concentrations in this experiment were not sufficiently high for this to be observed. The radicals H (n=3), H (n=4) and CH show almost constant trends as the reactions that form these radicals are independent of N₂ concentration. The trend shown by the C₂ radical decreases with increasing N₂ concentration. One possible explanation for this is the fact that with increasing CN concentration the amount of active carbon that forms C₂ decreases and hence these reactions are competing. Figure 11(d) shows a ratio plot with varying CH₄ concentration whilst keeping the concentration of N₂ constant at 6000 ppm. The NH radical in this case did not give sufficient reliable data over the range of pressures studied to show any trend and therefore was omitted from the ratio plot. The H (n=3)

and H ($n=4$) emissions follow similar trends for this plot, however they are not at the same ratio. This suggests that there is either a change in the electron density or the temperature of the electron gas that accompanies an increase in CH_4 concentration. The ratio of these two Balmer states depend upon these two properties because these excited states are produced by collisions between kinetically excited electrons and H atoms. With increasing CH_4 concentration there is an increase in the observed C_2 emissions due to the overall increase in active carbon within the plasma. The trend shown by the CH radical however shows a sharper initial increase, then a shallow increase thereafter. This is due to the fact that the reactions that produce CH and C_2 species are competing. Therefore initially, as there is a low concentration of C_2 , the CH radical reaction dominates. The CN radical follows a similar trend to that shown by the CH radical. An initial increase of CN is shown as CH_4 concentration increases but this then plateaus at higher CH_4 concentrations as competing reactions occur.

The experiments which were carried out using the low concentration N_2 gas mixture (1% N_2 in 99% H_2) are now discussed. These reactions contain a considerably lower concentration of N_2 and the nitrogen containing radical NH was not observed in all experiments.

Figure 12(a) shows a power plot for a $\text{N}_2/\text{CH}_4/\text{H}_2$ plasma at concentrations of 100 ppm N_2 and 4000 ppm CH_4 . All radicals within this plot show the same general trend which is to increase with increasing power. The trends shown here compare well with the high concentration case seen in figure 10(a). One notable difference between the high and low concentration cases is the gradient with which the observed NH increases. For the low concentration case the gradient is steeper than the high concentration case. One possible reason for this could be the reliability of the results, since the concentration of N_2 is considerably lower the signal from the optical emission spectrum is lower compared to the background and therefore is less reliable. Another explanation comes from the fact that at such low concentrations of N_2 there is less chance of a recombination reaction occurring and therefore there are less competing routes available to any N or NH_x (where $x > 1$) radicals within the plasma. However due to the fact that even for the high concentration case there is an abundance of H_2 compared to N_2 the second explanation becomes less likely.

Figure 12(b) shows a pressure plot for a $\text{N}_2/\text{CH}_4/\text{H}_2$ plasma at concentrations of 100 ppm N_2 and 4000 ppm CH_4 . In this case the NH radical was not observed due to the low concentrations of N_2 used. This plot compares well with the high concentration plot, 10(d) with the exception of the CN radical. In this case the observed CN radical stays relatively constant compared to the high concentration case. This is because of the low concentration of N_2 used, with increasing pressure the concentration of CH_4 is much greater than the concentration of N_2 .

Figure 12(c) shows a profile plot for a $\text{N}_2/\text{CH}_4/\text{H}_2$ plasma at concentrations of 200 ppm N_2 and 4000 ppm CH_4 . In this case the NH radical was not observed due to the low concentrations of N_2 used. The trends followed by observed radicals in this plot compares well with the high concentrations plots shown in figures 11(a) and 11(b). The peaks observed follow the same order as these cases.

Figures 13(a) and 13(b) show ratio plots for low N_2 concentration $\text{N}_2/\text{CH}_4/\text{H}_2$ plasmas. Due to the low concentration of N_2 used in these experiments the NH radical was unobserved in the optical emission spectra. Figure 13(a) shows the ratio for varying N_2 concentration with a constant

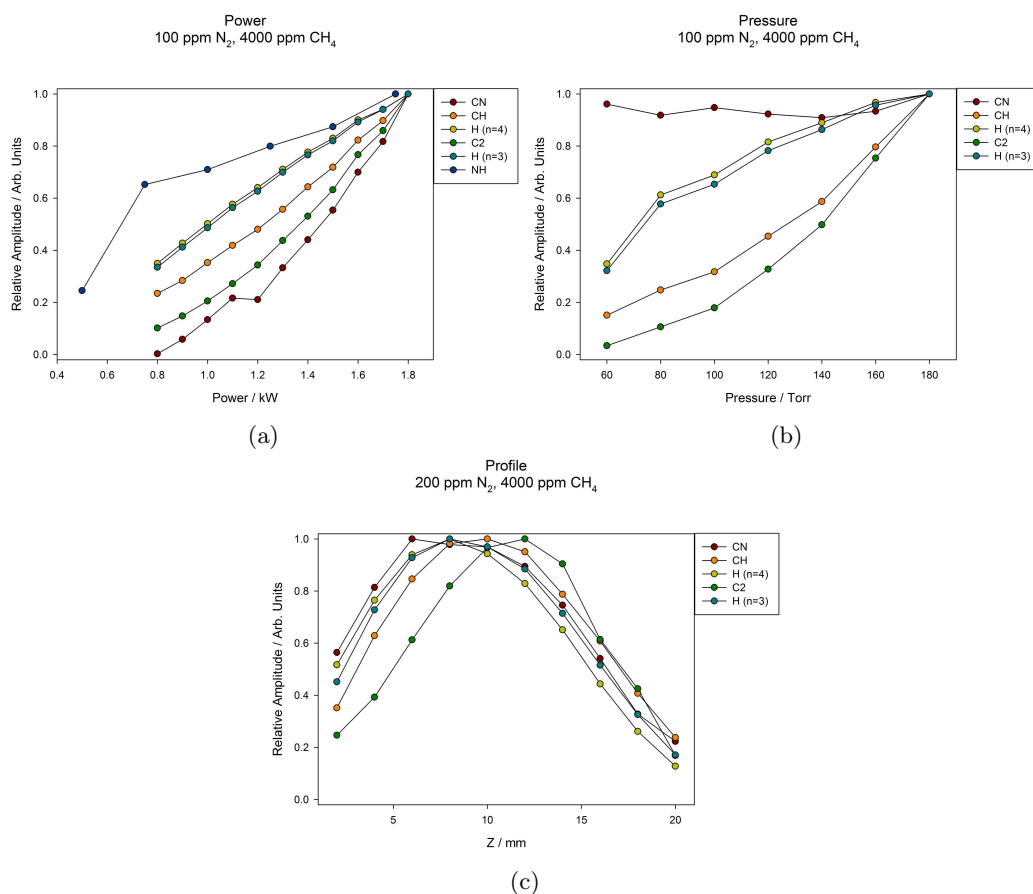


Figure 12: Three plots showing the results from three OES experiments. The measured parameter in each case is the relative amplitude which was calculated from the amplitude at each point divided by the maximum measured amplitude for each radical studied. Units for each plot are shown beside the axes and a legend for each data set within each graph is shown at the top right of each graph. (a) Shows a power plot of a N₂/CH₄/H₂ plasma at 100 ppm N₂ and 4000 ppm CH₄. (b) Shows a pressure plot of a N₂/CH₄/H₂ plasma at 100 ppm N₂ and 4000 ppm CH₄. (c) Shows a profile of a N₂/CH₄/H₂ plasma at 200 ppm N₂ and 4000 ppm CH₄.

CH₄ concentration of 4000 ppm. The CN radical here shows the same trend observed for the high concentration case in figure 11(c). There is a general increase in the observed CN OES signal with increasing N₂ concentration. H (n=3), H (n=4) and CH radicals remain constant over the range of N₂ concentrations studied while the C₂ amplitude increases. This is similar to the behaviour of these radicals for the aforementioned high concentration case in figure 10(c). One difference between the high concentration case and this low concentration case is that the signal shown by the C₂ radical shows opposite correlation with N₂ concentration. In this case the C₂ signal increases with increasing N₂ concentration. This suggests that the concentration of active carbon that forms both C₂ and CN species is dependant on the nitrogen concentration within the plasma. Figure

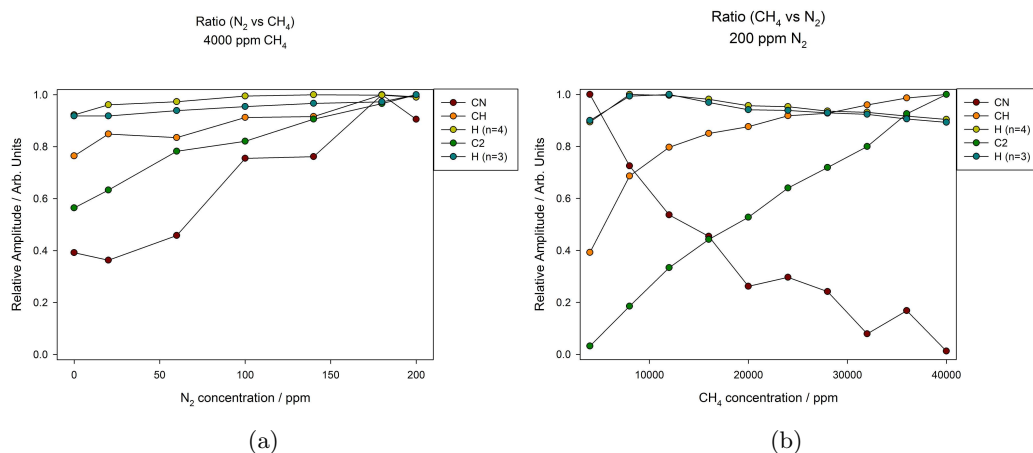


Figure 13: Two plots showing the results from two OES experiments. The measured parameter in each case is the relative amplitude which was calculated from the amplitude at each point divided by the maximum measured amplitude for each radical studied. Units for each plot are shown beside the axes and a legend for each data set within each graph is shown at the top right of each graph. (a) Shows a ratio plot of a N₂/CH₄/H₂ plasma varying the concentration of N₂ whilst keeping the concentration of CH₄ constant at 4000 ppm. (b) Shows a ratio plot of a N₂/CH₄/H₂ plasma varying the concentration of CH₄ whilst keeping the concentration of N₂ constant at 200 ppm.

13(b) shows the ratio for varying CH₄ concentration with a constant N₂ concentration of 200 ppm. The trends shown by the H (n=3), H (n=4) and CH radical signals agree with those found in the high concentration case in figure 11(d). However for the CN radical the opposite trend is shown, here there is a decrease in CN signal with increasing CH₄ concentration. This shows that, as there is an increase in the amount of C₂ in the plasma which is in competition with the CN radical, the CN radical is removed from the plasma. This is not the same for the high concentration case due to the lower concentration of active nitrogen within the plasma. Therefore there must be a maximum CN concentration in the plasma (which depends on the CH₄ concentration) because, in a large concentration of N₂, the signal from CN radicals is independent of CH₄ concentration. This because the maximum concentration has been reached. However for low concentrations this maximum has not been reached and therefore the CN and C₂ species are in direct competition.

Comparisons between the results presented here for low ppm nitrogen in carbon containing plasmas and those reported by Ma are of interest [22]. Ma presented the results from OES experiments with no nitrogen content for carbon and hydrogen plasmas with added argon. These experiments involved varying power, pressure and carbon flow rate in the same fashion as in this report. Small differences in trends can be seen for the data reported for profile experiments. Ma shows a similar peak value for the C₂ species but shows a lower peak value for the CH radical. This can be attributed to the change in electron properties within the plasma due to the added argon. However the trends shown by all other experiments are almost identical to those in this report. The significance of this is that there is little difference in the plasma chemistry between low concentrations of nitrogen and nominally nitrogen free plasmas. Therefore plasmas with nitrogen impurities introduced by either

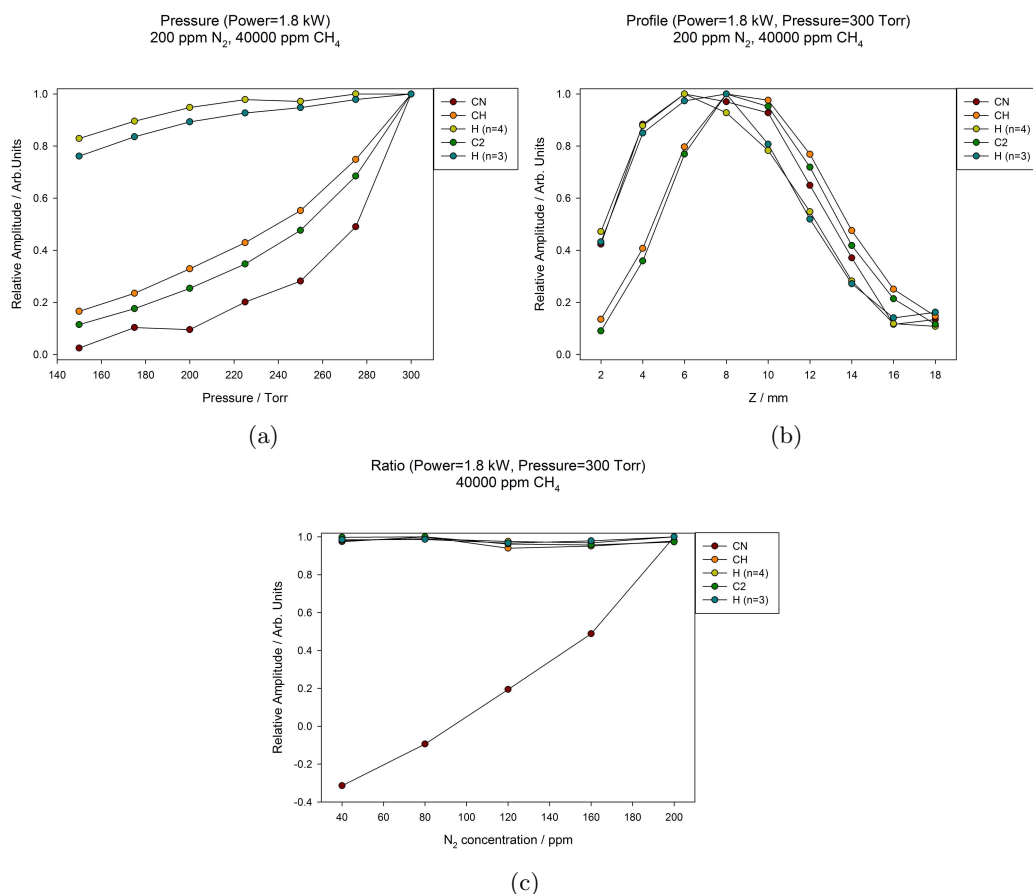


Figure 14: Three plots showing the results from Three OES experiments at powers and pressures greater than the standard values. The measured parameter in each case is the relative amplitude which was calculated from the amplitude at each point divided by the maximum measured amplitude for each radical studied. Units for each plot are shown beside the axes and a legend for each data set within each graph is shown at the top right of each graph. (a) Shows a Pressure plot of a N₂/CH₄/H₂ plasma at 200 ppm N₂ and 40000 ppm CH₄. (b) Shows a profile of a N₂/CH₄/H₂ plasma at 200 ppm N₂ and 40000 ppm CH₄. (c) Shows a ratio plot of a N₂/CH₄/H₂ plasma varying the concentration of N₂ whilst keeping the concentration of CH₄ constant at 40000 ppm.

by leaks in a reactor housing, impurities in input gas cylinders or other means will show the same trends as observed in this report.

The following paragraphs discuss OES experiments carried out using low concentrations of N₂ by using a nitrogen input gas consisting of 1% N₂ and 99% H₂. These experiments were carried out at pressures and powers higher than the standard discussed in sections 3.2.2 and 3.2.3. All data for the plots in figure 14 were carried out at 1.8 kW and the profile and ratio plots in this figure were carried out at 300 Torr of pressure. In each case the signal for the NH radical was not observed

and therefore is omitted from these plots. This absence of signal from the NH radical is forgiven by the motivation for studying high pressure and power conditions. This is to observe any changes in the CN chemistry under these conditions, these changes will be outlined in the coming paragraphs.

Figure 14(a) shows a pressure plot for high power. This was carried out for a $N_2/CH_4/H_2$ plasma with a N_2 concentration of 200 ppm and an CH_4 concentration of 40000 ppm. The range of pressures over which this was carried out starts and ends at greater values than the standard range discussed in section 3.2.3, running from 150 to 300 Torr. The trends shown by the CH and C_2 species are similar to those seen in the low power and pressure case in figure 12(a). These show a general increase with pressure up to high pressures due to an increase in the total concentration of CH_4 leading to an increase in active carbon. The trends shown by both the H (n=3) and H (n=4) species however do not agree with the low power and pressure case. Instead of increasing with a large gradient the signal from these two species level off at high pressures. This suggests that there is a maximum concentration of excited hydrogen atoms that can be formed from H_2 at any given power. The trend shown by the CN radical also differs to the low power and pressure case. Rather than remaining constant over the pressure range the signal from the CN radical increases with a large gradient. This is because whilst there is an increase in the total concentration of CH_4 there is not a significant increase H atoms within the plasma. Therefore the mechanisms that compete with the CN formation mechanism are hindered and hence the signal of the CN radical is observed to increase.

Figure 14(b) shows a profile at high pressure and power. This was carried out over the standard range for concentrations of 200 ppm N_2 and 40000 ppm CH_4 . The ordering of the peak value for the species studied here is as follows; CN emissions peak at 6 mm followed by CH and C_2 emissions which peak at 8mm, the centre of the plasma. The apparent difference in peak position for H (n=3) and H (n=4) emissions can be attributed to an error in measurement. This is justified by the identical trends shown before and after the peak position by both radicals. The ordering of the peaks in this case compare well with the low power and pressure case seen in figure 12(c) with the exception of the C_2 and CN peaks. Both of which are explained by the higher concentration of CH_4 used in this experiment.

Figure 14(c) shows a ratio plot at high pressure and power. This was carried out by varying the concentration of N_2 whilst keeping the concentration of CH_4 fixed at 40000 ppm. Since there is an abundance of hydrogen and carbon containing radicals within the plasma for this high concentration of CH_4 and the high values of power and pressure used. Only the species that depend on the overall nitrogen concentration are observed to change. The species; CH, H (n=3), C_2 and H (n=4) here remain constant over the concentration of N_2 since these do not depend on nitrogen. The CN species however increases with increasing N_2 as expected.

4.1.4 OES For NH_3 As An Input Gas

This section discusses OES experiments carried out using NH_3 as an input gas. As discussed in section 4.1.2 NH_3 is more efficient at producing active nitrogen within the plasma than the case where N_2 is used as an input gas.

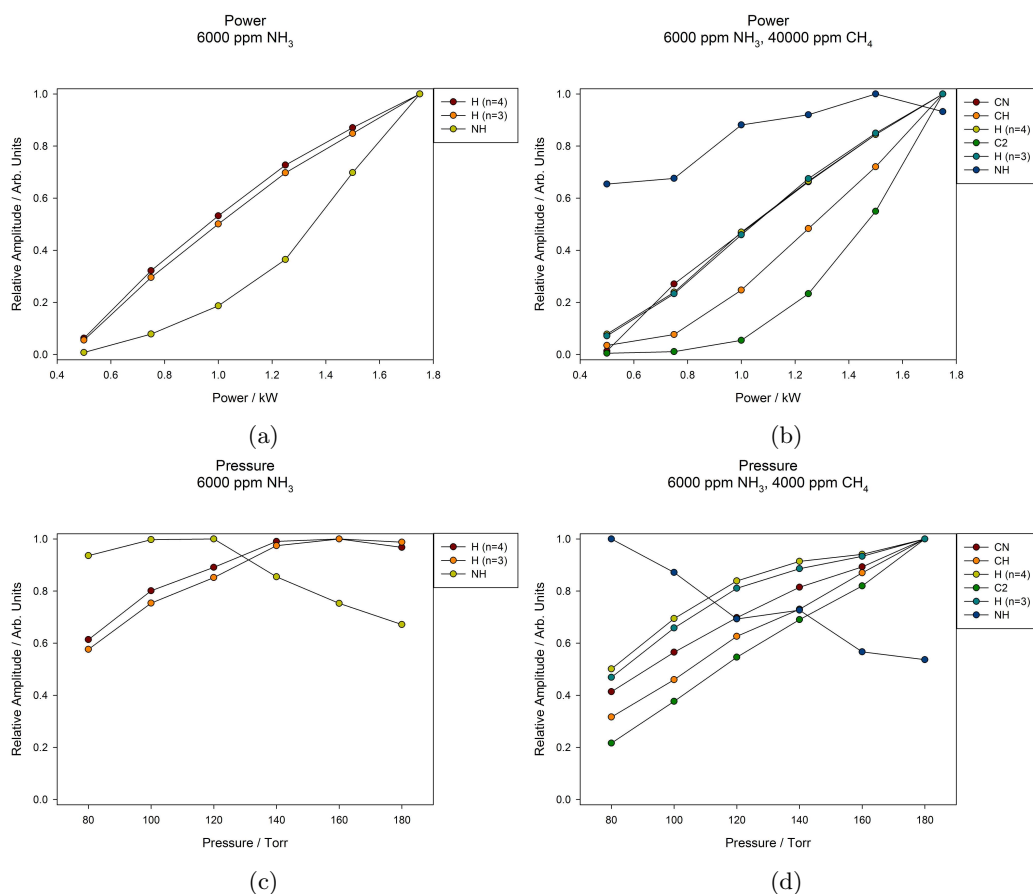


Figure 15: Four plots showing the results from four OES experiments. The measured parameter in each case is the relative amplitude which was calculated from the amplitude at each point divided by the maximum measured amplitude for each radical studied. Units for each plot are shown beside the axes and a legend for each data set within each graph is shown at the top right of each graph. (a) Shows a power plot of a NH₃/H₂ plasma at 6000 ppm NH₃. (b) Shows a power of a NH₃/CH₄/H₂ plasma at 6000 ppm NH₃ and 40000 ppm CH₄. (c) Shows a pressure plot of a NH₃/H₂ plasma at 6000 ppm NH₃. (d) Shows a pressure plot of a NH₃/CH₄/H₂ plasma at 6000 ppm NH₃ and 4000 ppm CH₄.

Figures 15(a) and 15(b) show power plots for both NH₃/H₂ and NH₃/CH₄/H₂ plasmas. Both of these were carried out at a constant NH₃ concentration of 6000 ppm and 15(b) was carried out at a constant concentration of CH₄ at 40000 ppm. For both of these plots the species that do not contain nitrogen show the same trends seen in the case where N₂ is used as the input gas; figures 10(a) and 10(c). For the NH₃/H₂ plasma one difference between this and the N₂ case can be seen. This is that the trends shown by the NH radical differ. For the N₂ case the trend shown is a linear increase with power, however that is not the case when using NH₃ as an input gas. The trend shown for the NH₃ case has a steeper dependence on power. This shows that for the NH₃ case

the abundance of NH in the plasma is dependant two factors that depend on the energy of the system. For example, since there is a higher amount of active nitrogen to form NH from the NH₃ gas then the reaction also depends on the amount of active hydrogen. Comparison to the N₂ case where there is a lower amount of active nitrogen with an abundance of active hydrogen shows that the limiting factor is the active nitrogen which increases with power. For figure 15(b) the only differing trend between this and the N₂ input gas case in figure 10(c) is that shown by the CN radical. The CN trend shown by the N₂ case is not linear whereas it is linear for the plot in figure 15(b). This is likely due to the fact that since NH₃ is used as the input gas there is an increase in the amount of active nitrogen within the plasma available to form the CN radical. Therefore the limiting factor in this reaction becomes the amount of active carbon which increases with power.

Figure 15(c) and 15(d) shows a pressure plot for both NH₃/H₂ and NH₃/CH₄/H₂ plasma respectively. Both of these were carried out at a constant NH₃ concentration of 6000 ppm and 15(d) was carried out at a CH₄ concentration of 4000 ppm. Both figures show the same trends for all radicals as their N₂ input gas counterparts seen in figures 10(b) and 10(d). Due to the fact that the measured variable in each case is the relative amplitude, the concentrations of each radical cannot be compared between these two plots. However due to the fact that NH₃ causes an increase in nitrogen containing radicals observed in section 4.1.2 it would be expected that if CRDS experiments were carried out measuring the column densities of the nitrogen radicals that are observed in the OES experiments the obtained values would be increased. Another advantage of using NH₃ in this case is that in figure 15(d) the trend of the NH radical is observed where as in figure 10(d) it was not. The trend shown by the NH radical in this case is a decrease in signal strength with increasing pressure. This is similar to the observed trend for the NH₃/H₂ and N₂/H₂ counterparts seen in figures 15(b) and 10(b). This decrease in signal is due to the competing reactions such as reactions that form CN radicals which is observed to increase with increasing pressure.

Figure 16 shows three profile plots for both NH₃/H₂ and NH₃/CH₄/H₂ plasmas. Each experiment was carried out at a concentration of 6000 ppm NH₃. Figure 16(a) shows the profile for a NH₃/H₂ plasma. The trends shown in this profile are as expected. The peak intensity for all species studied is at 8 mm above the substrate surface within the reactor. The trend shown by the NH radical follows the trends shown by the H (n=3) and H (n=4) species. This is because the signal from H (n=3) and H (n=4) species is related to the electron temperature and density within the plasma. The trends shown by all radicals other than NH in figure 16(b) are shared with the trends shown in the N₂ input gas counterpart seen in figure 11(a). The trend shown by the NH radical in this case shows a peak amplitude at 8 mm rather than the 4 mm previously observed. This is due to the fact that there is a higher concentration of active nitrogen in the case where NH₃ is used as an input gas rather than N₂. Therefore, while the reactions that form NH and CN are still in competition, the concentration of NH radicals overall is increased towards the centre of the plasma. This is also in part due to the fact that the concentration of CH₄ used in this experiment was 4000 ppm whereas in figure 11(a) 40000 ppm CH₄ was used. This contributes to the fact that the competition between CN and NH radicals is lessened due to the lower carbon content. Therefore the height at which there is a peak signal from NH radicals is dependant on both the active nitrogen and active carbon content inside the plasma. Figure 16(c) shows a profile plot at a higher concentration of CH₄; 40000 ppm CH₄. At these levels of carbon content the signal from the NH radical was unobserved. This is likely due to the fact that there is competition between the CN and NH reactions and therefore with a higher carbon content the concentration of NH within the plasma is not significant. The

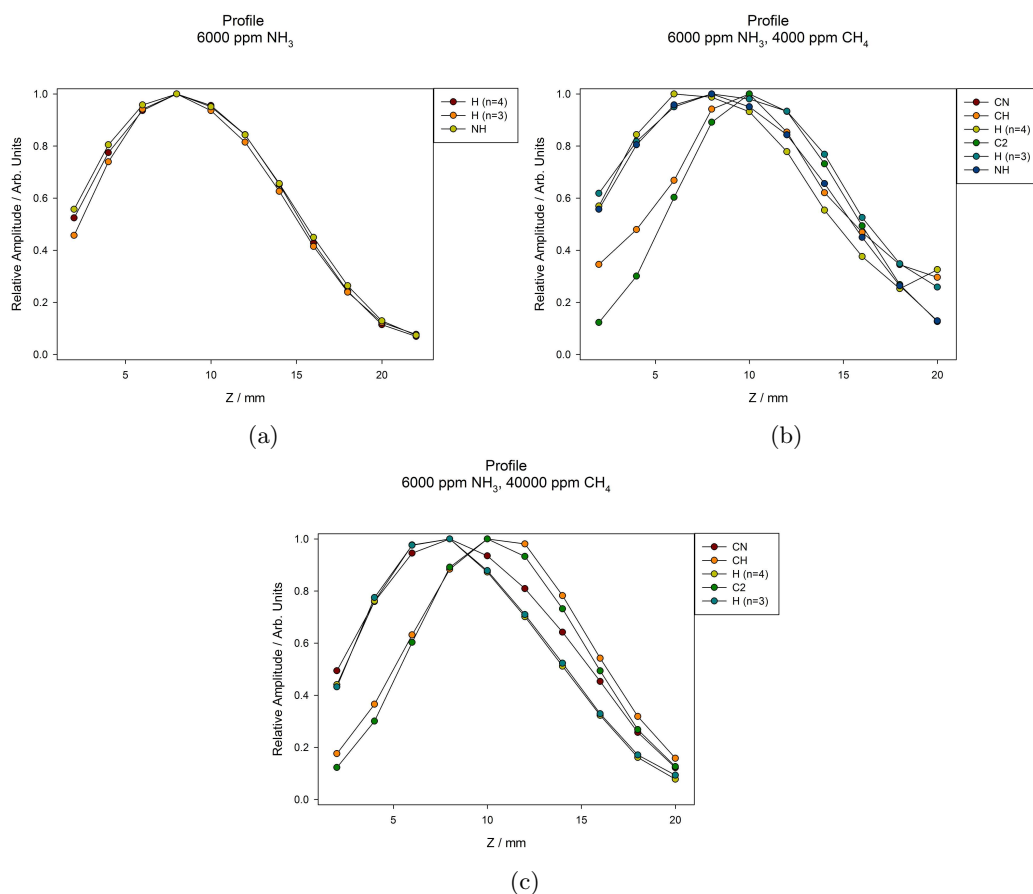


Figure 16: Three plots showing the results from Three OES experiments. The measured parameter in each case is the relative amplitude which was calculated from the amplitude at each point divided by the maximum measured amplitude for each radical studied. Units for each plot are shown beside the axes and a legend for each data set within each graph is shown at the top right of each graph. (a) Shows a profile of a NH_3/H_2 plasma at 6000 ppm NH_3 . (b) Shows a profile a $\text{NH}_3/\text{CH}_4/\text{H}_2$ plasma at 6000 ppm NH_3 and 4000 ppm CH_4 . (c) Shows a profile of a $\text{NH}_3/\text{CH}_4/\text{H}_2$ plasma at 6000 ppm NH_3 and 40000 ppm CH_4 .

trends shown by the other radicals agree with both the profile shown in figure 16(b) and those in figures 11(a) and 11(b).

Figure 17 show four ratio plots for both NH_3/H_2 and $\text{NH}_3/\text{CH}_4/\text{H}_2$ plasmas. Figure 17(a) shows a ratio plot for a NH_3/H_2 plasma. The trends for all the species studied in this experiment are as expected. Both H (n=3) and H (n=4) species remain constant throughout the experiment because the amount of hydrogen content within the plasma is always in abundance compared to the concentration of NH_3 . The signal from the NH radical increases linearly with increasing NH_3 concentration due to the increase in nitrogen content in the plasma. It should be noted that the trend shown here

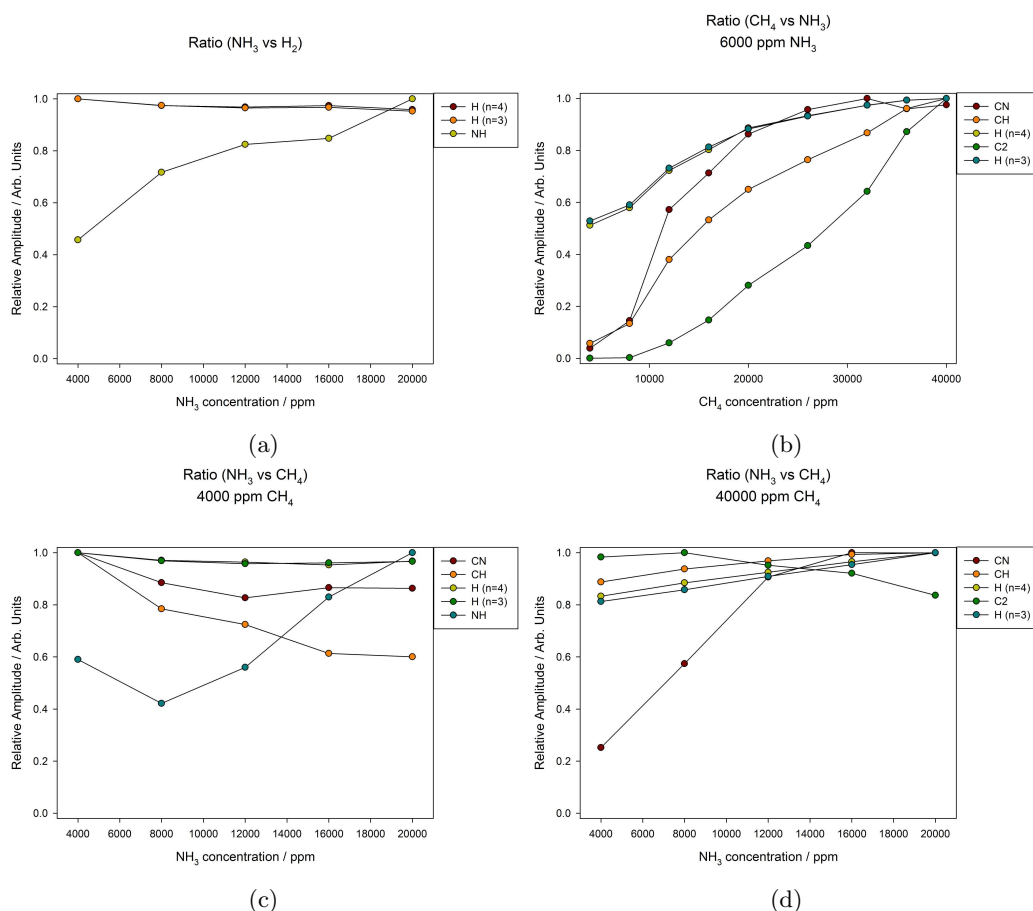


Figure 17: Four plots showing the results from four OES experiments. The measured parameter in each case is the relative amplitude which was calculated from the amplitude at each point divided by the maximum measured amplitude for each radical studied. Units for each plot are shown beside the axes and a legend for each data set within each graph is shown at the top right of each graph. (a), (b), (c) and (d) are all ratio plots. (a) is the plot of a NH_3/H_2 plasma varying the concentration of NH_3 . (b), (c) and (d) are plots of a $\text{N}_2/\text{CH}_4/\text{H}_2$ plasma. (b) varies the concentration of CH_4 whilst keeping the concentration of NH_3 constant at 6000 ppm. (c) varies the concentration of NH_3 whilst keeping the concentration of CH_4 constant at 4000 ppm. (d) varies the concentration of NH_3 whilst keeping the concentration of CH_4 constant at 40000 ppm.

directly correlates with the trend shown in the CRDS data for nitrogen hydrogen plasmas shown in sections 4.1.1 and 4.1.2 in figures 7(a) and 9(a). Figure 17(b) shows a ratio plot for a $\text{NH}_3/\text{CH}_4/\text{H}_2$ plasma at a constant NH_3 concentration of 6000 ppm. In this experiment an OES signal for the NH radical was not observed. The general trend shown by all species studied by OES for this experiment is an increase with increasing CH_4 concentration. This shows that the OES signal for all species studied depend upon the concentration of CH_4 within the plasma. It is unlikely that

the active hydrogen content significantly increases with an increase in CH_4 concentration for the range studied here. For a plasma which does not contain carbon the counter ion for the majority of the high temperature electrons in the electron gas are H_2^+ and H_3^+ . Upon the addition of CH_4 the dominant counter ions responsible become C_2H_2^+ and C_2H_3^+ which have lower ionization energies than H_2^+ and H_3^+ . This leads to an increase in the electron density and temperature of the electron gas. This is responsible for the increase in signals shown from all species with increasing CH_4 flow rate. The signal from carbon containing radicals studied; CN, CH and C_2 , will depend on both the electron properties of the plasma and the overall carbon content within the plasma. Therefore an increase with a greater gradient is observed for each of these species. Figure 17(c) shows the ratio for a $\text{NH}_3/\text{CH}_4/\text{H}_2$ plasma with a constant concentration of CH_4 at 4000 ppm. The signal for the C_2 species was unobserved and therefore has been omitted from this figure. The species CN, H (n=3) and H (n=4) remain relatively constant over the range of NH_3 concentrations studied. The signal from the CH radical shows an opposing trend to that shown by the signal from the NH radical. Therefore as the signal from the NH radical increases the signal from the CH decreases. Since the signals from both the H (n=3) and H (n=4) species remain constant over the NH_3 concentration range studied, the temperature of the plasma must remain relatively constant and therefore the trends shown by the NH and CH radicals are due to any increase or decrease in concentration of the species within the plasma. Therefore the reactions that form these two radicals are in competition with each other. Figure 17(d) shows a ratio plot for a $\text{NH}_3/\text{CH}_4/\text{H}_2$ plasma at a constant CH_4 concentration of 40000 ppm. This is a high concentration counterpart figure to the previous figure discussed: figure 17(c). For this figure the signal for the NH radical was undetected and therefore is not included. All radicals shown in this species other than the CN species show little change in signal over the concentration of NH_3 studied. The CN radical however shows an increase in signal with increasing NH_3 concentration. This is due to the initial high concentration of CH_4 allowing for a high concentration of CN to be produced as soon as the nitrogen concentration is increased.

4.2 Computational Results

The results for the incorporation of various nitrogen containing radicals are discussed in this section. The methods of computational calculation are discussed in section 3.4. Figures 18 and 20 show the reaction mechanisms for these incorporations. The enthalpies and activation energies for reactions that have been calculated in this section are reported to one significant figure. However the actual accuracy for the values, as discussed in section 3.4 is $\pm 10 \text{ kJ mol}^{-1}$. This section makes references to surface adducts, adduct species or simply adducts. These are surface radical carbons that has reacted with a species in the plasma to form a surface species that is not a terminating hydrogen or a carbon radical site. Structures (G), (C) and (M) from figure 18 and structures (H) and (C) from figure 20 are examples of C_9H_{13} clusters with surface adducts.

4.2.1 NH Radical Incorporation

The results from computational calculations on the incorporation of the N, NH and NH_2 radicals are shown in Figure 18. The starting point for any of the mechanisms shown is a C_9H_{14} diamond cluster (A), the calculated energy for which is $-922.2 \times 10^6 \text{ kJ mol}^{-1}$ (-351.3 A.U.). This then undergoes reaction with a hydrogen radical in the plasma to abstract one of the terminating hydrogen atoms. The abstraction of a terminating hydrogen (A-B) is shown as exothermic with a reaction enthalpy of -8.4 kJ mol^{-1} . However accounting for errors discussed in section 3.4 it is reasonable to

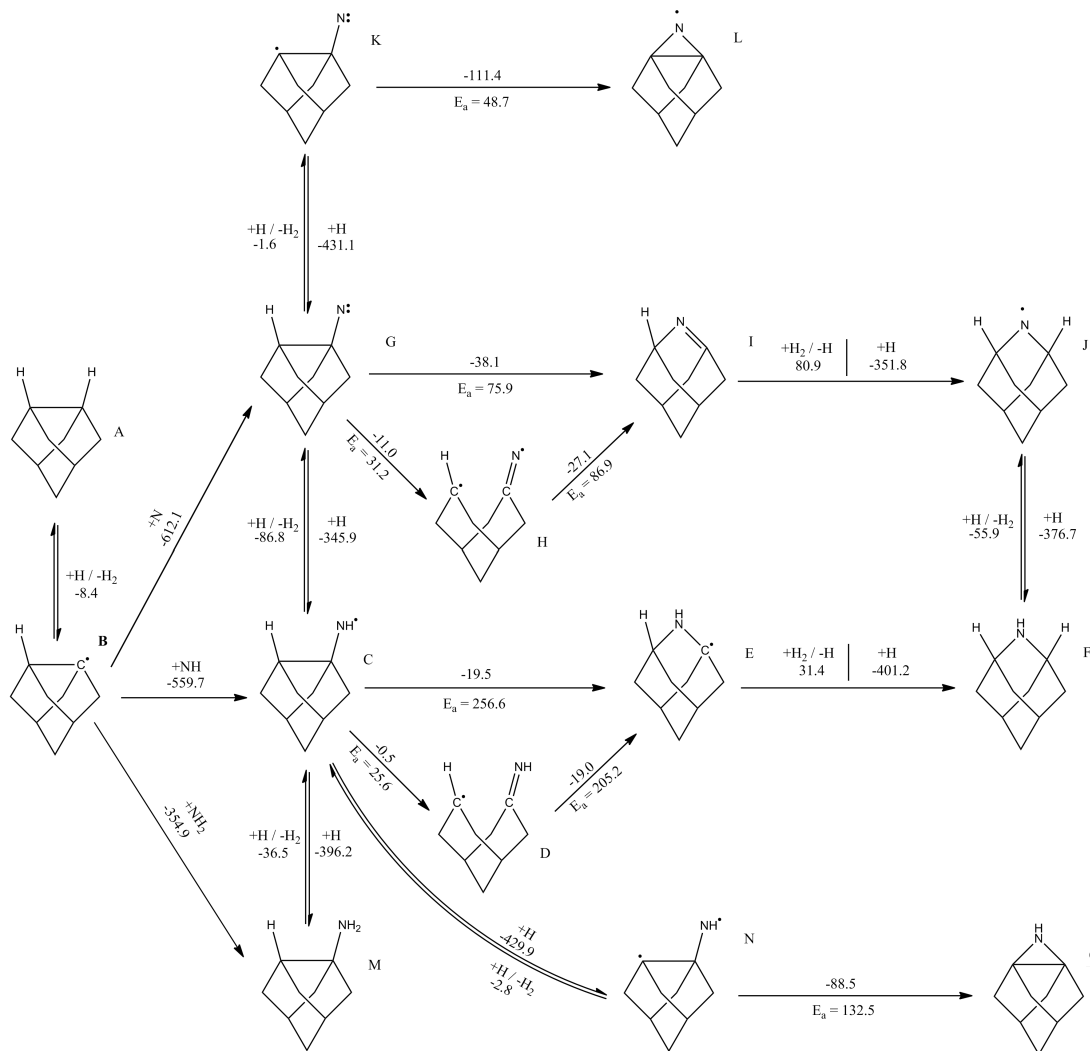


Figure 18: A schematic showing possible reaction mechanisms for the incorporation of the N, NH and NH₂ radicals into a C₉H₁₄ diamond cluster. Each arrow represents a reaction with reaction enthalpies denoted either with no label or with the reactants given. Activation energies E_a are also shown where applicable. All energies in this reaction scheme are given in kJ mol⁻¹. Reversible reactions with more than one possible set of reactants are shown with both reactants. The reverse of these reactions is then found by taking the negative of these numbers.

say that this reaction enthalpy is negligible. The relative energetics of this reaction are also shown in the first 2 steps of Figure 19. Considering that this reaction has a small reaction enthalpy it will proceed under the surface conditions and therefore there is a constant abstraction and addition of atomic hydrogen at the surface. This leads, with consideration of the number of times this reaction occurs, to a constant turnover of terminated and radical sites. Values for the frequency of these surface collisions have been calculated to be between 10⁴ and 10⁷ Hz [2]. This leads to a steady state surface radical concentration of 5 to 10 %.

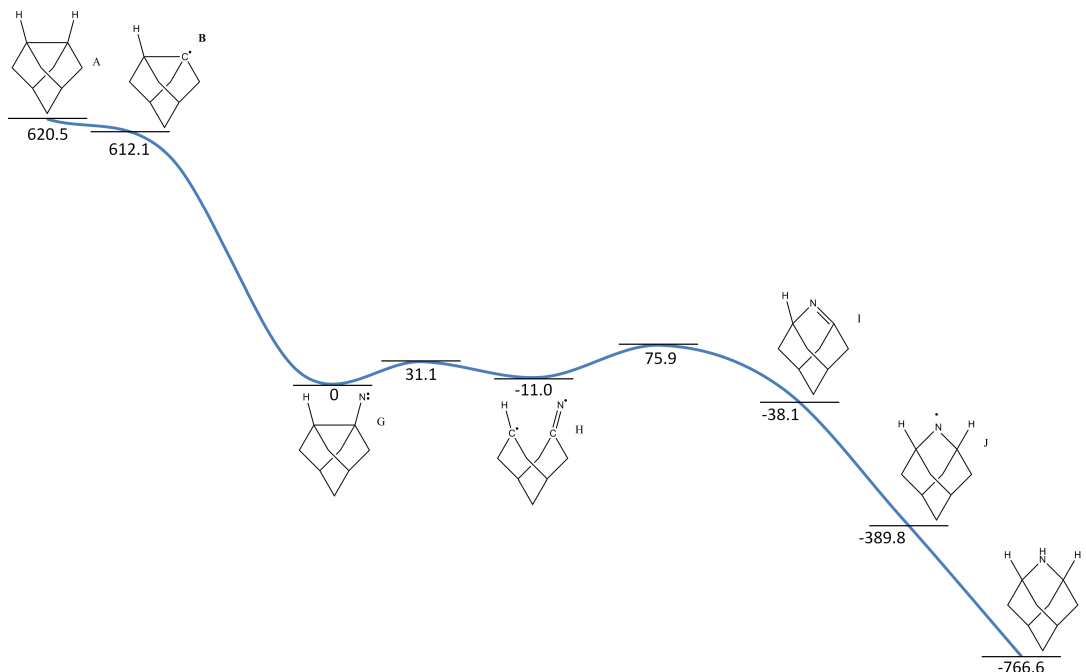


Figure 19: The incorporation mechanism (A–B–G–H–I–J–F) from figure 18 plotted to show the energetics of the mechanism. All energies are given in kJ mol^{-1} . The energy of the structure (G) is represented as 0 so that the energy of the structure (F) is given relative to the surface-radical starting point. Structures are shown for all steps, any markers without structures are intermediate activation energies.

Reaction (A-B) provides a surface radical with which any reactive species (H, N, NH, NH₂, CN and CNH studied in this project) found in a CVD plasma can easily add. These reactions are all expected to be exothermic with no activation barrier as they involve only bond making with no bond breaking. Addition of the three reactive nitrogen containing radicals for this scheme are exothermic for each case, as predicted, from the radical cluster (B) leading to the surface adducts (C), (G) and (M). The addition of the N radical is the most exothermic as it is the most unstable radical due to unpaired valence electrons, followed by NH and finally NH₂.

The surface adducts (from top to bottom) (K), (G), (C), (M) and (N) can be formed by reaction with gaseous species such as H and H₂. These reactions involve either an abstraction or addition of a terminating hydrogen atom. For example, abstraction of H from the NH adduct (C) by reaction with an H radical within the plasma can lead to either the adducts (G) or (N) depending upon which H is abstracted. Since each reaction between these 5 species (K), (G), (C), (M) and (N) has a route by which it is exothermic to abstract or add a terminating hydrogen it is expected that these adducts will be in equilibrium with each other. This will happen on a relatively quick time scale due to the frequency of hydrogen collisions with the surface previously discussed. These surface adducts can also be abstracted from the surface either by becoming highly vibrationally excited species through collisions or by reacting with a radical or molecule in the plasma. Both of

these methods can lead to the breaking of the surface-radical bond thereby extracting the radical. Finally another mechanism that these surface adducts can undergo, with the exception of the NH_2 radical cluster (M), is an incorporation by which the species forms a bridging species seen in the bridging clusters (L), (I), (E) and (O) (from top to bottom).

The reactions (C-E) and (G-I) both have exothermic reaction enthalpies, however the activation energies for the two are vastly different. For the reaction (C-E) the activation energy was calculated to be $256.6 \text{ kJ mol}^{-1}$. This is significantly greater than the predicted upper limit for a reaction to proceed; 100 kJ mol^{-1} (see section 3.4). It is therefore unlikely that the reaction (C-E) will proceed in one step. The reaction (G-I) however has a much lower activation energy of 75.9 kJ mol^{-1} which is lower than the predicted upper limit. For both these bridging reactions a ring opening method was also studied. These ring opening structures (D) and (H) are intermediate structures that were predicted to lower the overall activation energy. In both cases the intermediate ring opened structure has a lower activation barrier than the overall reaction. Both intermediate reactions are exothermic and have activation energies below 100 kJ mol^{-1} and therefore are likely to proceed under the surface conditions. Both reactions from the ring opened structure to the ring closed structures are exothermic. However the activation energies for these reactions vary greatly. For the reaction (D-E) the activation energy has a large value of $205.2 \text{ kJ mol}^{-1}$, greater than the 100 kJ mol^{-1} limit. Therefore the overall reaction (C-E), whether it proceeds by a ring opening method, or by a straight reaction is unlikely to proceed under the surface conditions of CVD diamond growth. This, however, is not the case for the reaction (H-I) where the activation energy, while greater than that of (G-I), is still less than the predicted upper limit at 86.9 kJ mol^{-1} . Therefore the overall reaction (G-I) is one possible mechanism by which a nitrogen radical can incorporate into a diamond surface. This ring opening and ring closing step is also shown in figure 19. This shows the favourable energetics discussed.

Once a radical has reached a ring closed structure, as discussed above, to completely incorporate it must react to form a fully hydrogen terminated structure. This is because there is a constant flux of hydrogen additions and abstractions at the surface. This leads to any species that can have additional terminating hydrogen atoms added undergoing addition reactions. Reactions (E-F) and (I-J) are examples of these. It has been previously discussed that the structure (E) is unlikely to form under standard conditions and so the reaction (E-F) is unlikely to happen due to the fact that (E) is unlikely to be formed. The reactions (I-J) and (J-F) are the likely steps that an incorporated nitrogen radical will follow to become fully terminated. The first reaction, (I-J), is exothermic on addition of a hydrogen radical from the surface but endothermic on reaction with a hydrogen molecule. This shows that the surface-hydrogen bond formed in (J) is less favourable than having a hydrogen molecule in the plasma. The implications of this are that this newly formed terminating hydrogen can be abstracted to form a hydrogen molecule in the plasma, much like the reaction (A-B) previously discussed. The reaction (J-F) shows the final termination step for an incorporated nitrogen radical. Both termination by hydrogen radical and hydrogen molecule are exothermic showing that the N-H bond formed is stable. The final steps in figure 19 show the favourable energetics of the steps (I-J-F) discussed here. Combined with the previously discussed steps in Figure 19, the overall incorporation from radical addition to full hydrogen termination can be seen with relative energies in context.

Other possible incorporation mechanisms were studied. These mechanisms require either the ab-

straction of a terminating hydrogen adjacent to a nitrogen containing radical, or the migration of the nitrogen containing radical across the surface until it meets a surface radical site. These both lead to the structures (K) for the case of a surface N radical and (N) for the case of a surface NH radical. The terminating hydrogen abstraction methods were studied and have been previously discussed as part of the interconversion reactions between (K), (G), (C), (M) and (N). The reactions (K-L) and (N-O) both involve a single ring closing step, both of which are exothermic. The reaction (K-L) has an activation energy of 48.7 kJ mol^{-1} which is below the predicted upper limit under surface conditions, this combined with the large exothermic reaction enthalpy of $-111.4 \text{ kJ mol}^{-1}$ lends confidence that this reaction would proceed. However, the limiting factor in this incorporation mechanism is the probability that a nitrogen radical attached to the surface would be next to a surface radical site at any one time. This must be taken into consideration when viewing the reaction (K-L) as a viable incorporation mechanism. The reaction (N-O) has an activation energy slightly greater than the predicted limit at $132.5 \text{ kJ mol}^{-1}$ which, when combined with the low probability of finding an NH radical attached to the surface next to a surface radical, means that this is an unlikely method of nitrogen radical incorporation.

4.2.2 CN Radical Incorporation

The results from the computational calculations of the CN and CNH radicals are shown in Figure 20. The structures (A) and (B) were not re-calculated and have the same energetics as in section 4.2.2. The first two steps shown in Figure 21 show the relative energetics of the reaction (A-B). The surface radical structure (B) then undergoes reactions with two nitrogen containing radicals studied in this section: CN and CNH. The reactions (B-C) and (B-H) are both exothermic and barrier-less since the processes only form bonds and break none. The reaction with CN has a reaction value of $-518.8 \text{ kJ mol}^{-1}$ which is more exothermic than that of the reaction with CNH which has a value of $-104.9 \text{ kJ mol}^{-1}$. The two adducts formed, (C) and (H), can undergo interconversion reactions by reacting with either gaseous hydrogen molecules or hydrogen radicals that exist within the plasma. Reactions with either of these reactants provide an exothermic route by which a surface CN radical can undergo an addition reaction to form CNH, or conversely a surface CNH radical can undergo an abstraction reaction to form CN. Further exothermic addition and abstraction reactions can lead to the formation of (K) and (M) which consist of nitrogen containing radicals attached to the surface adjacent to a surface radical site. Other possible mechanisms for the formation of the species (K) and (M) exist, one such mechanism is by migration of the nitrogen containing radical across the surface. Since there are exothermic routes for the interconversion between (K), (H), (C) and (M) (top to bottom) it is expected that they exist in equilibrium with each other. The equilibrium may be halted when one of these surface nitrogen containing radical species undergoes a reaction that either abstracts it from, or incorporates it into, the surface.

Incorporation mechanisms for CNH and CN radicals were studied in a similar manner to the NH and N incorporation in section 4.2.1, that is, both by a straight reaction and by a ring opening method. For the incorporation of a CN radical as seen in reaction (H-J) the straight reaction was found to be greatly endothermic with a value of $248.4 \text{ kJ mol}^{-1}$. Similar results were found for the ring opening mechanism, the reaction (H-I) was found to have an enthalpy of $+426.2 \text{ kJ mol}^{-1}$. The ring closing reaction (I-J) was then found to have an exothermic enthalpy with a value of $-177.8 \text{ kJ mol}^{-1}$. However due to the high reaction enthalpy of the ring opening step, the structure (I) is

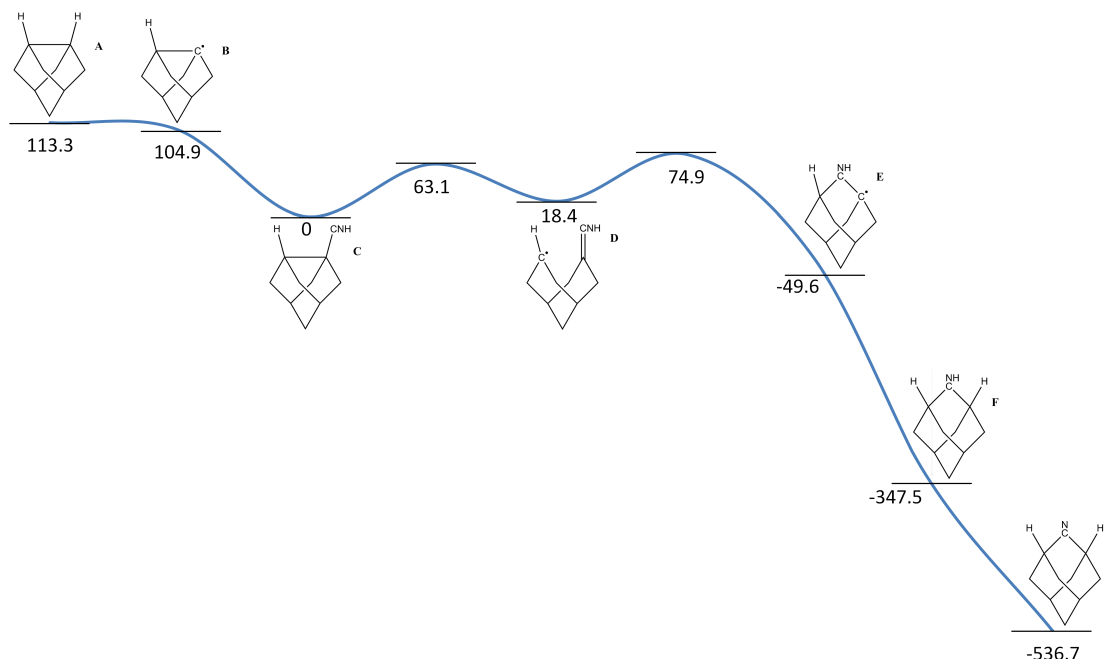


Figure 21: The incorporation mechanism (A–B–C–D–E–F–G) from figure 18 plotted to show the energetics of the mechanism. All energies are given in kJ mol^{-1} . The energy of the structure (C) is represented as 0 so that the energy of the structure (G) is given relative to the surface-radical starting point. Structures are shown for all steps, any markers without structures are intermediate activation energies.

opening mechanism for this step involves the reaction (C–D) which was found to be endothermic, however this is a relatively small enthalpy at $+18.4 \text{ kJ mol}^{-1}$. When considered with the errors discussed in 3.4 and the low activation energy of 63.1 kJ mol^{-1} it is still likely that this reaction will occur under the surface conditions. The ring closing reaction (C–D) is exothermic with a value of $-67.8 \text{ kJ mol}^{-1}$ and has a relatively low activation energy of 56.6 kJ mol^{-1} . It is therefore likely that, once the ring opened structure is achieved, the ring closing reaction will occur. Under the surface conditions within a CVD diamond growth environment both the routes (C–E) and (C–D–E) are of similar probability to occur. Once this CNH radical has been incorporated into a ring closed structure it can undergo further hydrogen radical addition reactions to form a fully terminated structure as seen in (F). The reaction with a hydrogen radical in the plasma is greatly exothermic with a value of $-298.0 \text{ kJ mol}^{-1}$. However the reaction with a hydrogen molecule is endothermic with a value of $134.7 \text{ kJ mol}^{-1}$ which means that the surface-hydrogen bond that is formed can also be abstracted from the surface at a later time. This is similar to the reaction (A–B). The hydrogen atom that terminates the incorporated CNH can also be abstracted to form the structure (G). From there it can also undergo an addition reaction to return to the fully terminated structure. It is likely that these two structures will exist in equilibrium. The entire incorporation mechanism discussed here can also be seen in figure 21 from surface-radical addition to full incorporation. This reaction mechanism is shown with energies relative to the structure (C).

The mechanism (C–O–B) shown is one possible abstraction method for a CNH radical attached to

the surface. This reaction is a beta-scission reaction that involves the exchange of a terminating hydrogen from a N-H bond in the CNH radical to a C-H bond. This gives an attached surface HCN molecule shown in (O). This re-arrangement reaction was found to have a small exothermic enthalpy of $-35.9 \text{ kJ mol}^{-1}$ however the activation energy was not found for this re-arrangement. The abstraction of this re-arranged structure (HCN, hydrogen cyanide) from the surface is endothermic with an enthalpy of 81.1 kJ mol^{-1} . These low enthalpy changes show that the reaction can occur however without the knowledge of the activation energy any comment on the rate of this reaction, and therefore its likelihood with respect to competing abstraction, conversion or incorporation reactions may not be accurate.

Ring closing reactions that involve a nitrogen containing radical attached to the surface adjacent to a surface radical site were studied. These reactions are seen in (K-L) and (M-N). Both these reactions form constrained and unsaturated (not fully terminated) structures. The reaction (K-L) was found to have a large and endothermic reaction enthalpy of $132.2 \text{ kJ mol}^{-1}$, combining this with the large activation energy of $411.8 \text{ kJ mol}^{-1}$, it is expected that this reaction will not proceed under surface conditions. The reaction (K-L) is therefore not a viable method for incorporation of a nitrogen containing radical. The reaction (M-N) has an exothermic reaction enthalpy of $-132.6 \text{ kJ mol}^{-1}$ but a relatively large activation energy of $138.9 \text{ kJ mol}^{-1}$. This activation energy is not significantly greater than the predicted upper limit for a reaction to proceed under surface conditions discussed in section 3.4 however given the fact that there are other possible routes for the structure (M) to take it is unlikely that this reaction is a viable incorporation method.

5 Conclusion

The results and discussion of the experiments carried out using cavity ring-down spectroscopy, optical emission spectroscopy and computational methods are summarized and concluded upon in this section.

The experimental data showed several significant results that will be discussed in the following paragraphs. The quantitative data given by the cavity ring-down spectroscopy experiments allowed the comparison between column densities, which are related to the concentration, of NH radicals within the plasma. It was observed that, for plasmas in the absence of carbon content, increasing the power used in experiments resulted in an increase in concentration of NH radicals within the plasma. This occurs due to an overall increase in the energy of atomic hydrogen species because the microwave power adsorbed by H_2 gas increases. Therefore there is a higher amount of H_2 dissociated and a higher amount of energy absorbed into rotational and vibrational states of H_2 . This increase in energy allows the nitrogen containing input gas to be broken down into its substitutions which then proceed to undergo a plethora of reactions, some of which produce the NH radical that was observed in experiments. This result differed between the two nitrogen containing gases studied; N_2 and NH_3 . For N_2 a significant increase was observed with an increase in power. This trend was also followed by the OES studies for an N_2 input gas in the conditions described. This result shows that there is an increase in NH concentration within the plasma but does not give quantitative data on the exact concentrations. However for the NH_3 gas the trend shown by the NH column density was either observed to stay relatively constant over the powers studied or was observed to increase to a lesser extent than the N_2 input gas case. This suggests that the energy required to reduce this

input gas to active nitrogen is less than when using N_2 . Therefore using NH_3 as an input gas would increase the active nitrogen content of the plasma. This observation is corroborated by the general increase in NH column density when comparing plots for N_2 as an input gas and NH_3 . Further experiments that may confirm and explore this result would include the study of other nitrogen containing species that exist in the plasma by cavity ring-down spectroscopy. The case of a nitrogen, carbon and hydrogen containing plasma showed similar results however, due to the increase in possible species from the addition of carbon the situation becomes increasingly complex. Simple trends for the column density of NH were not observed since the addition of carbon introduces competing reactions for nitrogen to follow that have an effect on the concentration of NH within the plasma. For example in figure 8(b) in section 4.1.2 the column density of NH is observed to decrease with power. This is due to an increase in competing reactions that reduce the overall concentration of NH within the plasma. Ratio experiments support this. For example figure 7(b) shows that, with decreasing CH_4 concentration and increasing N_2 concentration there is an overall increase in the concentration of NH radicals within the plasma. Figures 9(a) and 9(b) show excellent examples for the fact that there are competing reactions for the NH radical formation. In figure 9(a) a NH_3/H_2 plasma is used the column density of NH observed at 4000 ppm NH_3 is $1.64 \times 10^{12} \text{ cm}^{-2}$, in this case there are no competing reactions from carbon due to the fact that there is no carbon in the plasma. However when carbon is introduced in the form of CH_4 input gas the column density at this NH_3 concentration decreases to a value of $1.17 \times 10^{12} \text{ cm}^{-2}$. Further study into this effect could involve the CRDS study of species formed by these competing reactions. OES studies carried on the CN radical which is in competition with the NH radical allow the comparisons between trends but not the direct comparison of the concentrations of these two species. Another result is shown by the ratio plots for nitrogen and hydrogen only plasmas shown in figures 7(a) and 9(a). This is that, in the abundance of hydrogen the concentration of NH radicals within the plasma is proportional to the concentration of nitrogen containing gas introduced at constant power and pressure.

The general trend shown by CRDS pressure experiments (figure 6(b)) show an increase in NH column density with increasing pressure. As explained this is simply due to an increase in the total number of radicals present in the plasma which is attributed to the increase in the total density of N_2 within the reactor. The OES pressure studies show similar trends for both nitrogen and hydrogen only plasmas and for nitrogen, carbon and hydrogen plasmas. There is a general increase in the signal from all species studied. Since one of the contributing factors to the signal produced in an OES experiment is the concentration of species within the plasma the increase in signal here can be attributed to the increase in species concentration. It should be noted, however, that the NH signal from the OES experiments of this type can be observed to decrease in figures 10(b), 15(c) and 15(d). It was discussed that there were two possible contributing factors to this. One compared the plateau in H ($n=3$) and H ($n=4$) species with the decrease in NH signal giving evidence for a mechanism that prevented the production of NH species by an increase of H_2 molecules within the plasma. The second addressed the issue with the NH signal from OES experiments depending upon the temperature, electron temperature and electron density of the plasma.

Profile experiments carried out both by CRDS and OES methods showed one general shape. This is a low signal at values of Z close to the substrate surface which increased towards the centre of the plasma which was observed to be located at 8 mm above the surface. The signal then decreased as the outer regions of the plasma were probed. The observation that the centre of the plasma was located at 8 mm lends confidence to choosing 8 mm as the standard height at which power, pressure

and ratio plots were carried out. The main feature of these plots was the variation in the peak height for each species studied. The CRDS experiments gave insight into the spatial distribution of the NH radical in a more accurate manner than the OES experiments. This is because over the height of the plasma the temperature within the plasma changes. This has a substantial effect on the emissions observed by OES. For the CRDS data obtained using N_2 as an input gas for both; nitrogen and hydrogen only, and nitrogen, carbon and hydrogen plasmas, the height at which the highest concentration of NH radicals was observed was at 8 mm above the surface. This corresponds to the centre of the plasma. This is because this is the hottest region within the plasma and therefore, as previously discussed, since the energy required to break the N_2 bond is relatively high, this is the expected region to contain the highest concentration of nitrogen reaction precursors. This result however was different when using NH_3 as an input gas. For NH_3 the range over which NH radicals were at a high concentration was increased. This is because the energy required to break the NH_3 molecule into substitution components is less than for N_2 and therefore this decomposition reaction is observed to occur over a wider spatial distribution.

Comparisons between low and high pressured OES data gave insight into the composition of the plasma with vastly varying conditions. An initial observation was that at high pressures with constant power there is a value at which the amount of hydrogen atoms produced by dissociation by microwave excitation reaches a maximum. That is to say that the power of microwaves used to dissociate hydrogen reaches a maximum. This is shown by the plateau in H (n=3) and H (n=4) species observed at high pressures (figure 14(a)) compared to the increase in H (n=3) and H (n=4) signals observed at lower pressures (figure 12(b)). Another observation made from the high pressure and power OES experiments was that the concentration of CN radicals within the plasma is proportional to the nitrogen content within the plasma. This is shown in the ratio plot in figure 14(c) where all other radicals studied remained constant over the the concentration range studied due to the high pressure and power and only a change in the CN signal was observed. Since the ratio of the other radicals does not change over the N_2 concentration range the factors, other than concentration, that affect the optical emission from the plasma, remain constant. Therefore the only changing feature for this plot is the nitrogen content of the plasma. Comparisons between work presented in this report for low concentrations of nitrogen were also compared with those for nominally nitrogen free plasmas presented by Ma [22]. The comparisons showed that, for low nitrogen content the trends shown by non carbon containing radicals were essentially the same as for no nitrogen content. This is important as in almost all CVD plasmas nitrogen impurities within the plasma cannot be avoided. Therefore, since low concentrations of nitrogen show the same trends as no nitrogen content plasmas the nitrogen impurities should make no difference to the plasma chemistry.

The computational data discussed in section 4.2 showed many significant results with respect to the mechanisms for incorporation of various nitrogen containing radicals at the surface. In each calculation a C_9H_{14} diamond cluster was used as a starting point for each surface study. As discussed in section 3.4 the use of this small structure with respect to a larger structure is justified as it provides an accurate energy compared to a larger structure but the computational expense of calculations on this scale are significantly less. The error in results presented for computational calculations was discussed in section 3.4 and was given as $\pm 10 \text{ kJ mol}^{-1}$. It was found that the formation of surface radicals, that is a surface carbon radical where a terminating hydrogen has been abstracted, were of negligible enthalpy change and therefore were likely to occur under the conditions at the

surface in a CVD reaction environment. This led to the conclusion that there is a constant surface coverage of these surface radicals which may be terminated either to form the hydrogen terminated site or terminated with another species within the plasma. All terminations that were calculated within this experiment were found to be exothermic. This is because the formation of bonds with no bond breaking is exothermic. Surface adducts, not to be confused with surface radicals, are surface radicals that have been terminated with a species that attacks from the plasma. These surface adducts were studied for nitrogen species that are related by hydrogen. For example N, NH and NH₂ radicals are related by the addition or abstraction of hydrogen. These addition or abstraction reactions were found to all have exothermic mechanisms. This was found for the interconversion of N, NH and NH₂ as well as CN and CNH (not to be confused with HCN). Therefore the N, NH and NH₂ species were in equilibrium with each other, the rate of which depends upon the rate of hydrogen collisions with the surface. This was also found for the CN and CNH surface adducts. This gives each surface adduct three possible types of reaction that can lead to a change at the surface. These are abstractions, interconversions previously discussed and incorporations which are now discussed. For the NH radical incorporation two methods gave results suggesting that they provide likely mechanisms for the incorporation into the diamond surface. These formed an unsaturated constrained structure, which can be seen in structure L in figure 18 and a saturated unconstrained structure seen in structure (F) in the same figure. The mechanism by which structure (L) was formed was a simple ring closing step from structure (K), a nitrogen adduct. This has an enthalpy of -111.3 kJ mol⁻¹ and an activation energy of 48.7 kJ mol⁻¹. The mechanism by which structure (F) was formed can follow either a straight mechanism, (G-I), or by a ring opening mechanism (G-H-I). The energetics of the first mechanism consisted of an enthalpy of -38.1 kJ mol⁻¹ with an activation energy of 75.85 kJ mol⁻¹. The energetics of the second mechanism consisted of an initial enthalpy of -11.0 kJ mol⁻¹ with an initial activation energy of 31.2 kJ mol⁻¹ to form the ring opened structure which was then followed by a final enthalpy of -27.1 kJ mol⁻¹ with a final activation energy of 86.9 kJ mol⁻¹. Both of these lead to the unterminated structures (I) and (J), the latter of which exists within equilibrium with the fully terminated incorporated surface radical structure (F). The energetics of this incorporation mechanism were presented in figure 19. Similar results were found for the study of radical incorporation for the species CN and CNH. One likely mechanism discussed was the incorporation of a surface terminating CNH species (structure (C)) which incorporated by either a straight mechanism or a ring opening mechanism to form the structure (E). The former of these was calculated to react with an enthalpy of -49.5 kJ mol⁻¹ and an activation energy of 75.8 kJ mol⁻¹. The latter underwent an initial ring opening step to form the structure (D) with an enthalpy of 18.4 kJ mol⁻¹ and an activation energy of 63.1 kJ mol⁻¹ followed by a ring closing step which was calculated to have an enthalpy of -67.9 kJ mol⁻¹ and an activation energy of 56.6 kJ mol⁻¹. In a similar mechanism to the NH incorporation case, the full incorporation from the structure (E) to the structure (G) involved several hydrogen addition steps. The structures (F) and (E) were found to exist in equilibrium with each other depending on collisions with hydrogen in the plasma.

The following paragraphs discuss future work for experiments for diamond CVD using N/C/H plasmas. These experiments would mostly involve expanding upon the experiments already carried out in this and other reports.

In this report the results from CRDS experiments were presented and analysed for the NH radical within the plasma. It is also possible to study other nitrogen containing radicals using the

same CRDS method used in this report. Success has been shown in the measurement of the CN column density by CRDS methods [23]. This radical was studied by OES in this report but the absolute concentration of the species was not discussed. Comparisons between the column densities of the NH radical presented in this report and those of the CN radical would give insight into the mechanisms of their competing reactions. Power, pressure, profile and ratio experiments should be carried out, as for this report, on the CN radical. The increase in signal shown by the CN radical in the OES experiments at high pressure and power should be reproduced by the CN radical column density in equivalent CRDS experiments. Confirmation of this would prove that an increase in power and pressure results in an increase in the concentration of CN in the plasma and that this is the cause of the increase in OES signal rather than an increase in electron density and temperature.

This report presents the results from computational modelling of the surface chemistry in a CVD environment. There has been a large amount of research into the modelling of the gas phase chemistry that occurs within the plasma. This allows the prediction of the distribution of species within the plasma, many of which cannot easily be measured by spectroscopic techniques such as CH_3 [4]. Models of plasmas with different input gases such as argon and oxygen have been carried out [24] [25]. Modelling can also produce information of different properties of a plasma such as dissociation rates of input gases [26]. Therefore modelling a N/C/H plasma is a logical step towards understanding the processes, specifically competing reactions, that occur in a variety of different conditions. This will allow for quantitative analysis of the distribution of species throughout plasma which can be compared with CRDS data from this report and future CRDS experiments on different radicals.

The computational experiments carried out in this report give insight into the incorporation of radicals into a growing diamond surface during a CVD process. However the incorporation of a radical is only a small part of its contribution to the overall growth of thin films. Further computational approaches are needed in order to fully understand the growth process at the surface. One proposed experiment should include the migration of the surface adducts studied in this report across the surface, specifically to step edges where the diamond changes plane from [100] and [111]. This experiment would give insight into the difference in nitrogen content in the bulk of the diamond for [100] and [111] planes which was briefly discussed in section 2.2. Another experiment would involve migration of surface adducts across a surface until they meet with another surface adduct. If the mobility of nitrogen containing adducts is greater than that of hydrocarbon adducts then this could provide evidence for an increase in growth rate discussed in section 2.2. Another experiment which could provide insight into the increased growth rate would be to migrate a hydrocarbon adduct to a stable, fully incorporated and terminated nitrogen adducts such as (F) in figure 18 and (F) in figure 20. If a the migrated adduct forms a stable, immobile species with either of these adducts then this could become a nucleation centre for diamond growth. Eventually a computational goal should be the study of diamond growth over these proposed nucleation sites, i.e. the growth of a new layer.

References

- [1] W. Eversole *U.S. Patents 3030187. 3030188*, 1962.

- [2] J. E. Butler, Y. A. Mankelevich, A. Cheesman, J. Ma, and M. N. R. Ashfold, "Understanding the chemical vapor deposition of diamond: recent progress," *Journal of Physics: Condensed Matter*, vol. 21, no. 36, p. 364201, 2009.
- [3] J. R. Rabeau, P. John, J. I. Wilson, and Y. Fan, "The role of C_2 in nanocrystalline diamond growth," *Journal of Applied Physics*, vol. 96, no. 11, pp. 6724–6732, 2004.
- [4] Y. A. Mankelevich, M. N. R. Ashfold, and J. Ma, "Plasma-chemical processes in microwave plasma-enhanced chemical vapor deposition reactors operating with C/H/Ar gas mixtures," *Journal of Applied Physics*, vol. 104, no. 11, p. 113304, 2008.
- [5] J. E. Butler, R. L. Woodin, L. M. Brown, and P. Fallon, "Thin film diamond growth mechanisms," *Philosophical Transactions of the Royal Society of London. Series A: Physical and Engineering Sciences*, vol. 342, no. 1664, pp. 209–224, 1993.
- [6] J. C. Angus, A. Argoitia, R. Gat, Z. Li, M. Sunkara, L. Wang, and Y. Wang, "Chemical vapour deposition of diamond," *Philosophical Transactions of the Royal Society of London. Series A: Physical and Engineering Sciences*, vol. 342, no. 1664, pp. 195–208, 1993.
- [7] A. Cheesman, J. N. Harvey, and M. N. R. Ashfold, "Computational studies of elementary steps relating to boron doping during diamond chemical vapour deposition," *Phys. Chem. Chem. Phys.*, vol. 7, pp. 1121–1126, 2005.
- [8] A. Cheesman, J. Harvey, and M. Ashfold, "Studies of carbon incorporation on the diamond [100] surface during chemical vapour deposition using density functional theory," *Journal of Physical Chemistry, A*, vol. 112, pp. 11436 – 11448, 2008. Publisher: American Chemical Society.
- [9] T. Liu and D. Raabe, "Influence of nitrogen doping on growth rate and texture evolution of chemical vapor deposition diamond films," *Applied Physics Letters*, vol. 94, no. 2, p. 021119, 2009.
- [10] R. Locher, C. Wild, N. Herres, D. Behr, and P. Koidl, "Nitrogen stabilized [100] texture in chemical vapor deposited diamond films," *Applied Physics Letters*, vol. 65, no. 1, pp. 34–36, 1994.
- [11] A. Chayahara, Y. Mokuno, Y. Horino, Y. Takasu, H. Kato, H. Yoshikawa, and N. Fujimori, "The effect of nitrogen addition during high-rate homoepitaxial growth of diamond by microwave plasma cvd," *Diamond and Related Materials*, vol. 13, pp. 1954 – 1958, 2004. Proceedings of the 9th International Conference on New Diamond Science and Technology (ICNDST-9).
- [12] W. Muller-Sebert, E. Worner, F. Fuchs, C. Wild, and P. Koidl, "Nitrogen induced increase of growth rate in chemical vapor deposition of diamond," *Applied Physics Letters*, vol. 68, no. 6, pp. 759–760, 1996.
- [13] R. Samlenski, C. Haug, R. Brenn, C. Wild, R. Locher, and P. Koidl, "Incorporation of nitrogen in chemical vapor deposition diamond," *Applied Physics Letters*, vol. 67, no. 19, pp. 2798–2800, 1995.

- [14] P. May, P. Burridge, C. Rego, R. Tsang, M. Ashfold, K. Rosser, R. Tanner, D. Cherns, and R. Vincent, "Investigation of the addition of nitrogen-containing gases to a hot filament diamond chemical vapour deposition reactor," *Diamond and Related Materials*, vol. 5, no. 35, pp. 354 – 358, 1996. International Journal on the Science and Technology of Diamond and Related Materials. Proceedings of the 6th European Conference on Diamond, Diamond-like and Related Materials Part 1.
- [15] J. A. Smith, J. B. Wills, H. S. Moores, A. J. Orr-Ewing, M. N. R. Ashfold, Y. A. Mankelevich, and N. V. Suetin, "Effects of NH_3 and N_2 additions to hot filament activated CH_4/CH_2 gas mixtures," *Journal of Applied Physics*, vol. 92, no. 2, pp. 672–681, 2002.
- [16] T. Vandavelde, T. Wu, C. Quaeys, J. Vlekken, M. Dolieslaeger, and L. Stals, "Correlation between the oes plasma composition and the diamond film properties during microwave p-cvd with nitrogen addition," *Thin Solid Films*, vol. 340, no. 12, pp. 159 – 163, 1999.
- [17] J. Ma, J. C. Richley, M. N. R. Ashfold, and Y. A. Mankelevich, "Probing the plasma chemistry in a microwave reactor used for diamond chemical vapor deposition by cavity ring down spectroscopy," *Journal of Applied Physics*, vol. 104, no. 10, p. 103305, 2008.
- [18] A. Cheesman, J. A. Smith, M. N. R. Ashfold, N. Langford, S. Wright, and G. Duxbury, "Application of a quantum cascade laser for time-resolved, in situ probing of CH_4/H_2 and $\text{C}_2\text{H}_2/\text{H}_2$ gas mixtures during microwave plasma enhanced chemical vapor deposition of diamond," *The Journal of Physical Chemistry A*, vol. 110, no. 8, pp. 2821–2828, 2006.
- [19] J. Ma, A. Cheesman, M. N. R. Ashfold, K. G. Hay, S. Wright, N. Langford, G. Duxbury, and Y. A. Mankelevich, "Quantum cascade laser investigations of CH_4 and C_2H_2 interconversion in hydrocarbon/ H_2 gas mixtures during microwave plasma enhanced chemical vapor deposition of diamond," *Journal of Applied Physics*, vol. 106, no. 3, p. 033305, 2009.
- [20] A. J. Hallock, E. S. F. Berman, and R. N. Zare, "Direct monitoring of absorption in solution by cavity ring-down spectroscopy," *Analytical Chemistry*, vol. 74, no. 7, pp. 1741–1743, 2002.
- [21] M. D. Wheeler, S. M. Newman, A. J. Orr-Ewing, and M. N. R. Ashfold, "Cavity ring-down spectroscopy," *J. Chem. Soc., Faraday Trans.*, vol. 94, pp. 337–351, 1998.
- [22] J. Ma, *Exploration of the gas phase chemistry in microwave activated plasmas used for diamond chemical vapour deposition*. PhD thesis, University of Bristol, 2008.
- [23] R. L. Stolk and J. J. T. Meulen, "Cavity ring down spectroscopy measurements of absolute CN concentrations during flame deposition of diamond," *The Journal of Chemical Physics*, vol. 117, no. 18, pp. 8281–8291, 2002.
- [24] J. C. Richley, O. J. L. Fox, M. N. R. Ashfold, and Y. A. Mankelevich, "Combined experimental and modeling studies of microwave activated $\text{CH}_4/\text{H}_2/\text{Ar}$ plasmas for microcrystalline, nanocrystalline, and ultrananocrystalline diamond deposition," *Journal of Applied Physics*, vol. 109, no. 6, p. 063307, 2011.
- [25] J. R. Petherbridge, P. W. May, and M. N. R. Ashfold, "Modeling of the gas-phase chemistry in C–H–O gas mixtures for diamond chemical vapor deposition," *Journal of Applied Physics*, vol. 89, no. 9, pp. 5219–5223, 2001.

- [26] K. Tachibana, M. Nishida, H. Harima, and Y. Urano, "Diagnostics and modelling of a methane plasma used in the chemical vapour deposition of amorphous carbon films," *Journal of Physics D: Applied Physics*, vol. 17, no. 8, p. 1727, 1984.